Energy Research and Development Division
FINAL PROJECT REPORT

IMPROVING THE UNDERSTANDING OF $PM_{2.5}$ AND OZONE CHEMISTRY FROM AIR QUALITY MONITORING FOR MORE ACCURATE PREDICTION OF POWER GENERATION IMPACTS

Prepared for: California Energy Commission
Prepared by: Lawrence Berkeley National Laboratory

MARCH 2013
CEC-500-2014-015

PREPARED BY:

Primary Author(s):
Nancy Brown
Ling Jin

Lawrence Berkeley National Laboratory
1 Cyclotron Rd.
Berkeley, CA 94720
510-486- 4241

Contract Number: 500-09-036

Prepared for:

California Energy Commission

Marla Mueller
Contract Manager

Linda Spiegel
Office Manager
Energy Generation Research Office

Laurie ten Hope
Deputy Director
ENERGY RESEARCH AND DEVELOPMENT DIVISION

Robert P. Oglesby
Executive Director

DISCLAIMER

This report was prepared as the result of work sponsored by the California Energy Commission. It does not necessarily represent the views of the Energy Commission, its employees or the State of California. The Energy Commission, the State of California, its employees, contractors and subcontractors make no warranty, express or implied, and assume no legal liability for the information in this report; nor does any party represent that the uses of this information will not infringe upon privately owned rights. This report has not been approved or disapproved by the California Energy Commission nor has the California Energy Commission passed upon the accuracy or adequacy of the information in this report.

ACKNOWLEDGEMENTS

The authors would like to thank Dr. Ajith Kaduwela, Mr. Bruce Jackson, Dr. Jeremy Avise, and Dr. Jin Lu of the Air Resources Board for their assistance in obtaining emission inputs and boundary conditions. We would also like to thank our French student intern Nathaniel Seror for his modeling and data collection work. We thank our sponsors, the California Energy Commission, for supporting this research.

PREFACE

The California Energy Commission Energy Research and Development Division supports public interest energy research and development that will help improve the quality of life in California by bringing environmentally safe, affordable, and reliable energy services and products to the marketplace.

The Energy Research and Development Division conducts public interest research, development, and demonstration (RD&D) projects to benefit California.

The Energy Research and Development Division strives to conduct the most promising public interest energy research by partnering with RD&D entities, including individuals, businesses, utilities, and public or private research institutions.

Energy Research and Development Division funding efforts are focused on the following RD&D program areas:

- Buildings End-Use Energy Efficiency
- Energy Innovations Small Grants
- Energy-Related Environmental Research
- Energy Systems Integration
- Environmentally Preferred Advanced Generation
- Industrial/Agricultural/Water End-Use Energy Efficiency
- Renewable Energy Technologies
- Transportation

Improving the Understanding of $PM_{2.5}$ and Ozone Chemistry from Air Quality Modeling for More Accurate Prediction of Power Generation Impacts is the final report for the More Accurate Prediction of Generation Impacts through Better Characterization of Particulate Matter and Ozone Chemistry project (contract number 500-09-036) conducted by Lawrence Berkeley National Laboratory. The information from this project contributes to Energy Research and Development Division's Energy-Related Environmental Research Program.

For more information about the Energy Research and Development Division, please visit the Energy Commission's website at www.energy.ca.gov/research/ or contact the Energy Commission at 916-327-1551.

ABSTRACT

California's San Joaquin Valley is out of compliance with both fine particulate matter and ozone standards. Particulate matter and ozone controls are traditionally considered separately because their high pollution periods are not concurrent on seasonal timescales. Ozone concentrations are high in the summer and fine particulate matter concentrations are high in the winter. The late summer and early fall also contribute significantly to the exceedances of annual fine particulate matter standards when ozone levels are high. Utility loads are also at their highest during this time period. This goal of this study was to control the two pollutants together during the late summer and early fall period by applying the United States Environmental Protection Agency's Community Multiscale Air Quality photochemical air quality model to central California for the August-September period of years 2000 and 2005. Particulate nitrates were found to be the main secondary component in fine particulate matter mass. The formation chemistry of particulate ammonia nitrate was limited by the availability of nitric acid. Higher ozone and fine particulate matter were found to occur together during late summer and early fall under more stagnant conditions. Nitrogen oxides control was most effective for reducing fine particulate matter and it would also begin to benefit ozone control as emissions were reduced further.

Keywords: Particulate matter, ozone, late summer early fall, central California, sensitivity analysis

Please use the following citation for this report:

Brown, Nancy; Ling Jin. (Lawrence Berkeley National Laboratory). 2013. ***Improving the Understanding of $PM_{2.5}$ and Ozone Chemistry from Air Quality Modeling for More Accurate Prediction of Power Generation Impacts.*** California Energy Commission. Publication number: CEC-500-2014-015.

TABLE OF CONTENTS

Acknowledgements i

PREFACE ii

ABSTRACT iii

TABLE OF CONTENTS iv

LIST OF FIGURES v

LIST OF TABLES vi

EXECUTIVE SUMMARY 1

Introduction 1

Project Purpose 1

Project Results 1

Project Benefits 2

CHAPTER 1: Introduction 3

CHAPTER 2: Modeling Data and Methods 6

2.1 Model Inputs 6

2.2 Observational Data 8

2.3 Analysis Methods 10

2.3.1 Paired Analysis Methods for Model Evaluation 10

2.3.2 Correlation Analysis 10

2.3.3 Sensitivity Analysis 11

CHAPTER 3: Base Year Simulations and Model Performance 13

3.1 Spatial and Temporal Distribution of Simulated Ozone and $PM_{2.5}$ 13

3.2 Paired Performance Metrics 14

3.3 Modeled vs Observed PM Composition 16

CHAPTER 4: Temporal Relationship between Ozone and $PM_{2.5}$ 18

4.1 Pearson Correlation 18

4.2 Partial Correlation 19

CHAPTER 5: Ozone and $PM_{2.5}$ Responses to Emission Controls 22

5.1 Meteorological Effects on Concentrations and Chemical Coupling 22

5.2 Meteorology vs Emission Effects on Ozone 26

CHAPTER 6: Conclusions 29

GLOSSARY 31

REFERENCES 33

APPENDIX A: Emission Quality Checking and Processing A-1

APPENDIX B: Lateral Chemical Boundary Conditions B-1

LIST OF FIGURES

Figure 1: Modeling Domain (SARMAP) Indicated by Purple Rectangle. 6
Figure 2: Spatial Distribution of Emissions (mol/day): Anthropogenic VOC (AVOC), NOx, Biogenic VOC (BVOC, and Ammonia (NH3) 7
Figure 3: Monitoring Locations 9
Figure 4: Afternoon Sea Surface Pressure (100 Pa) and Temperature (K) Anomalies (Relative to the Seasonal Mean) Averaged over the Two Episodes 11
Figure 5: Period Averages for (a) Maximum 8 h Average O_3, (b) 24 h Average $PM_{2.5}$, (c) Log of Adjusted Gas Ratio (AdjGR) 13
Figure 6: Diurnal Profiles of $PM_{2.5}$, Components, O_3 and Gaseous HNO_3 Averaged over Locations with $PM_{2.5}$ >15 ug/m^3 in Figure 5 14
Figure 7: Modeled vs Observed PM Species at the Four Monitoring Network Locations. 15
Figure 8: Modeled vs Observed $PM_{2.5}$ Composition at IMPROVE Sites (Remote). 16
Figure 9: Modeled vs Observed $PM_{2.5}$ Composition at STN Sites (Urban). 17
Figure 10: Statistical Distribution of Hourly and Daily Correlation Coefficients between Ozone and $PM_{2.5}$ 18
Figure 11: Statistical Distribution of Hourly and Daily Correlation Coefficients between Ozone and $PM_{2.5}$ Species 19
Figure 12: Conceptual Framework of Potential Meteorological Effects on Nitrates and Ozone .. 20
Figure 13: Partial Correlation Coefficients between O_3, PM, and Meteorological Variables on Hourly (upper) and Daily (Lower) Timescales 20
Figure 14: Episode Averaged 8h Ozone Maxima (Left) and 24h Average $PM_{2.5}$ (Right) for August (Upper) and Sep (Lower) Episodes for Year 2005 23
Figure 15: Episode Averaged Semi-Normalized First Order Sensitivity of 8h Ozone Maxima to AVOC and NO_x Emissions and S^1 Sensitivities of 24h Average $PM_{2.5}$ to NOx Emissions for August (Upper) and September (Lower) Episodes in Year 2005 24
Figure 16: Hourly O_3 and $PM_{2.5}$ Sensitivities to AVOC (Left) and NOx (Right) Averaged for August (Upper) and September (Lower) Episodes of Year 2005 at "High PM Locations". The PM Sensitivities are Further Decomposed into Sensitivities of PM Components to AVOC and NO_x. 25

Figure 17: Hourly $PM_{2.5}$ Sensitivities to Ammonia (Upper) and SOx (Lower) Emissions Averaged for August (Left) and September (Right) Episodes of Year 2005 at "High PM Locations". The PM Sensitivities are Further Decomposed into PM Components with Same Legend as in Figure 16 26
Figure 18: Cumulative Distribution of 8h Max O_3 over High PM Locations. Vertical Lines Correspond to 60 ppb (Possible Future O_3 Standard), and 75 ppb (Current O_3 Standard) 27
Figure 19: Distribution of O_3 to NO_x Sensitivities over High PM Locations for Different Ozone Levels. The Median (Horizontal Line) in Each Box Indicates a Central Tendency of the Distribution 28
Figure 20: Average 8h Max O_3 over High PM Locations with Reduction (Percent) of NO_x of Year 2005 Level 28

LIST OF TABLES

Table 1 Annual Average of $PM_{2.5}$ per Site per Year (ug/m^3) 3
Table 2: Quantities for Calculating Temporal Correlations of Daily and Hourly Time Scales 10
Table 3: Meteorological Conditions of the Two Episodes 12
Table 4: Common Precursor Emissions (Averaged over Mondays) 27

EXECUTIVE SUMMARY

Introduction

Particulate matter (PM) and ozone controls are traditionally considered separately because their high pollution periods are not concurrent on seasonal timescales. California's San Joaquin Valley is out of compliance with both $PM_{2.5}$ (particle mass with diameters less than 2.5 microns) and ozone standards. Ozone concentrations are high in the summer and $PM_{2.5}$ concentrations are high in the winter. The late summer and early fall also contribute significantly to the exceedances of annual $PM_{2.5}$ standards when ozone levels are high. Utility loads are also at their highest during this time period.

Project Purpose

This goal of this study was to examine the possibility of controlling the two pollutants together during the late summer and early fall period by applying the United States Environmental Protection Agency's (EPA's) Community Multiscale Air Quality (CMAQ) photochemical air quality model to central California for the August-September period of years 2000 and 2005.

Project Results

The CMAQ model August-September simulations of base year 2000 were evaluated with observations obtained from various networks. The CMAQ model predicted total $PM_{2.5}$ better than its speciated components due to compensating errors. Particulate nitrates were the main secondary component in 24-hour $PM_{2.5}$ mass and were dominated by morning and nighttime contributions. Ammonia nitrate formation was limited by the availability of gaseous nitric acid.

Ozone and $PM_{2.5}$ were negatively associated on an hourly basis largely due to opposite effects of diurnal variations in relative humidity and temperature. Eight-hour ozone maxima and 24-hour average $PM_{2.5}$ were positively associated on daily timescales because both were sensitive to the Planetary Boundary Layer height (an indication of atmospheric stagnation). These findings indicated that higher ozone and $PM_{2.5}$ tended to occur together during late summer and early fall under more stagnant conditions and that it was important to consider control of these two pollutants in concert.

Nitric acid formation was coupled to ozone chemistry by sharing the same precursor compounds, oxides of nitrogen (NO_x) and anthropogenic volatile organic compounds. The chemical coupling of PM and ozone was investigated by simulating responses of the two pollutants to their common precursor emissions over two episodes representative of ventilated and stagnant conditions, respectively. Both concentrations and their sensitivities to precursor emissions of the two pollutants were greater in magnitude under the more stagnant conditions. $PM_{2.5}$ sensitivities were dominated by sensitivities of particulate ammonia nitrate to NOx. The formation of nitric acid was limited by NO_x and NO_x control was found to be most effective for controlling particulate ammonia nitrate.

Higher ozone levels (greater than 75 parts per billion) during the more stagnant episode at high PM locations could also benefit NO_x control, but in general ozone and PM largely showed opposite responses to NO_x for the emissions considered here (year 2000 and year 2005). NO_x

control on average became beneficial for both pollutants as NO_x emissions were reduced further (about 15 percent for stagnant conditions and about 30 percent for ventilated conditions from the year 2005 level).

Project Benefits

This study explored ways to reduce fine particular matter and ozone concentrations. Fine particular matter causes adverse health effects, so reducing these concentrations could benefit the overall health of California residents, especially those residents prone to chronic respiratory problems.

CHAPTER 1: Introduction

The California Central Valley is out of compliance with both the annual (15 ug/m^3) and the new standard of 12 ug/m^3) and the 24-hour (35 ug/m^3) fine particulate matter ($PM_{2.5}$) standards. Extensive modeling studies have been analyzed to demonstrate that the most effective, if not only, strategy for achieving compliance is to reduce nitrogen oxides (NO_x) emissions dramatically. The formation of particulate matter (PM) is complex and involves many precursors and pathways. Between 50 and 75 percent of the PM mass occurs during the period from November through January (Chow et al., 2006); however, the summer and early fall also contribute significantly to exceedances of the annual and 24-hour PM standards, when utility loads are at their highest. Since meteorology is such an important factor in the large wintertime loading, and limits the effectiveness of source control, one strategy for decreasing the annual average is to reduce the summertime loading to values as low as possible. With peak demand continuing to increase in the summer and early fall, understanding the best options for meeting the growing power demands and minimizing the air quality impact is of upmost importance.

Recently, the San Joaquin Valley Unified Air Pollution Control District (SJVUAPCD) has provided data summarizing annual average $PM_{2.5}$ data for 11 sites in the valley for a nine-year period (Table 1), as well as data for 24-hour $PM_{2.5}$. Fresno and Bakersfield exceed the annual and 24 hour standards. The data indicate that as you move further south, the annual $PM_{2.5}$ concentrations increase. Examination of a time series of total PM mass revealed many days with concentrations in excess of the annual standard and some days with concentrations in excess of the 24-hour standard in August and September for the Years 2000 through 2008 with a higher number of such days in September. This time period coincides with periods when utility loads are highest.

Table 1 Annual Average of $PM_{2.5}$ per Site per Year (ug/m^3)

County	Monitoring Site	2000	2001	2002	2003	2004	2005	2006	2007	2008
San Joaquin	Stockton-Hazelton	15.4	13.8	16.6	13.5	13.2	12.4	13.0	12.9	14.3
Stanislaus	Modesto-14th Street	18.7	15.5	18.6	14.4	13.5	13.8	14.8	14.9	15.9
Merced	Merced-M Street	16.6	14.4	18.7	15.6	15.1	14.0	14.8	15.2	*
Fresno	Clovis-Villa	16.3	18.0	16.1	18.4	16.3	16.3	16.4	16.4	15.3
Fresno	Fresno-1st	*	19.8	21.5	17.7	16.3	16.6	16.7	18.8	17.3
Fresno	Fresno-Hamilton & Winery	18.4	18.6	21.2	17.8	16.9	16.9	17.6	16.8	16.5
Kings	Corcoran-Patterson Ave	16.3	19.1	21.4	16.2	17.4	17.4	16.8	18.3	15.7
Tulare	Visalia-Church Street	23.9	22.4	23.2	18.2	17.0	18.8	18.7	20.3	19.8
Kern	Bakersfield-Planz	20.2	20.8	23.5	17.8	17.4	19.8	19.3	21.7	23.4
Kern	Bakersfield-	22.5	21.1	22.6	17.1	18.8	17.9	18.7	21.9	21.9

	California									
Kern	Bakersfield-Golden	22.6	21.8	24.0	19.6	18.1	19.1	18.6	19.9	17.8

* no sufficient data.

Ozone and PM have traditionally been considered as separate pollution problems, especially for central California because their concentrations are not correlated temporally on an annual basis. Speciation of $PM_{2.5}$ revealed that the largest contributors to mass during the summer and fall period were carbonaceous aerosol and ammonium nitrate (NH_4NO_3), which is formed via gas phase reactions between ammonia (NH_3), emitted from agriculture sources, and nitric acid (HNO_3). The nitrate (NO_3) forms from NO_x, which is emitted from mobile, area, and point sources including power generation. In the central valley, NH_4NO_3 formation is HNO_3 limited, which means NH_4NO_3 concentrations decrease with decreases in HNO_3. Although daytime chemistry is assumed to contribute one fourth of the nitric acid, questions remain about the mechanism affecting the remainder of its production (Minejima et al., 2009). Since a major fraction of $PM_{2.5}$ forms from atmospheric gas-to-particle conversion, attempts to reduce $PM_{2.5}$ would require control of the same volatile organics and nitrogen oxides emissions that are also precursors to ozone formation. Characterization of temporal correlations between ozone and $PM_{2.5}$ in the late summer-early fall can provide useful information for the design of multi-pollutant control strategies as well as information to determine pollution exposure.

The objective of this study is to use United States Environmental Protection Agency's (US EPA) new Community Multiscale Air Quality model (CMAQ v4.7) (Foley et al. 2010) to understand better the formation of $PM_{2.5}$ and ozone concentrations in Central California for periods in August and September for a recent year, and to determine their sensitivities to precursor compounds, especially those emitted during power generation. The model year is a recent one where reliable emissions are developed that has meteorology typical of the region. The new model, CMAQ v4.7, includes full gas phase chemistry, improved treatments of Secondary Organic Aerosol (SOA) formation (Carlton et al. 2010), improved dinitrogen pentoxide (N_2O_5) chemistry (Davis et al. 2008), improved mass transfer (Kelly et al. 2009), as well as other improvements that enable us to predict both ozone and $PM_{2.5}$ with acceptable accuracy.

Much of the prior work in the area of PM modeling has focused on the winter periods commensurate with the California Regional Particulate Air Quality Study (CRPAQS) and has used different models or earlier versions of CMAQ. This study uses a different model, a different model year, a different modeling period, and emphasizes the impact of power generation on the two pollutants.

Aerosol modeling is more complex than ozone modeling since aerosol formation depends on the following: (1) meteorology, (2) emissions of gas phase and aerosols, (3) the aerosol size distribution and dynamics, and (3) gas phase and heterogeneous chemistry (Byun and Schere, 2006). We focus on fine particles ($PM_{2.5}$) including: primary and secondary organic particles, black or elemental carbon, NH_4NO_3, and ammonium sulfate (NH_4SO_4). The model assumes that the fine particles are in equilibrium with the ambient gas and vapor phase species at the ambient relative humidity and form aqueous solutions. The ISORROPIA model (Nenes et al. 1998) is used to calculate thermodynamic equilibrium between organic aerosol species and gas-

phase concentrations. Key algorithms simulating aerosol processes in CMAQ include: (1) aerosol removal by size dependent dry deposition; (2) aerosol-cloud droplet interactions and removal by precipitation; (3) new particle formation by binary homogeneous nucleation in the sulfuric acid-water vapor systems; (4) the production of organic aerosol components from gas phase precursors; and (5) particle growth via coagulation and condensation. Fortunately, the formation of secondary organic aerosols in CMAQ allows one to distinguish between anthropogenic and biogenic sources. There are recent improvements involving the sectional method, which is used to calculate aerosol production by size classes. Aerosol modeling is very computationally intensive; CMAQ 4.7 brings more complexity regarding the chemistry and physical processes important to aerosol formation without hugely enhanced computational complexity.

Meteorology plays a large role in determining pollutant concentrations. There are five important circulation processes in the Central Valley that are consistent from year to year (Bao et al., 2008): (1) the incoming low level marine flow through the Carquinez Strait in the Sacramento River Delta, (2) the diurnal cycle of upslope/downslope flows, (3) the up and down valley flow in the Sacramento Valley (SV), (4) the nocturnal low level jet in the San Joaquin Valley (SJV), and (5) the orographically induced mesoscale eddies. The summer meteorology is driven by heating that creates a thermal low pressure system and a large onshore pressure gradient between the coast and the desert.

Our previous study has captured these effects; hence we will use these meteorological fields since central valley meteorology has been shown to be quite consistent from year to year. These meteorological fields have been benchmarked against observations (See Michelson et al. 2010 and Jin et al. 2010). Sensitivity calculations are performed for representative meteorological conditions that are selected based on our previous studies (Jin et al. 2011, 2012). This also reduces some of the computational burden because sensitivity calculations are also computationally intense.

Chapter 2 provides a description of the research methods and modeling data used in the simulations conducted in this study. The base year (year 2000) simulations and model performance evaluation are presented in Chapter 3. In Chapter 4, we analyze the spatial and temporal behaviors of simulated ozone and fine particulate matter concentrations and their relationships using correlation analysis. In Chapter 5, we simulate ozone and $PM_{2.5}$ responses to precursor emission controls under two representative meteorological conditions using emissions from year 2005. We summarize our findings and recommend future research in Chapter 6.

CHAPTER 2:
Modeling Data and Methods

2.1 Model Inputs

The study domain (the so-called San Joqauin Valley Regional Modeling Adaptation Project - SARMAP domain) is a sub-region (34.5 to 39°N and 118.5 to 123°W) of the domain selected for the Central California Ozone Study, which consists of several geographically divided air basins labeled in Figure 1. The SJV is surrounded by the Sierra Nevada and coastal ranges. On typical summer days, westerly winds are funneled into the central valley through gaps in coastal ranges with large portions of the flow directed into SJV. Therefore, the San Francisco Bay area (SFB) and SV are the major upwind SJV emission sources. Two busy highways run through the SJV: Highway 99 connects the major urban centers, and Interstate 5 runs through rural and agricultural areas. Air basins are labeled on the map for SFB, SV, Mountain County (MC), SJV, North and South Central Coast (NCC and SCC). The SJV is further divided into three parts (Northern, Middle, and Southern part) by the dashed lines.

Figure 1: Modeling Domain (SARMAP) Indicated by Purple Rectangle.

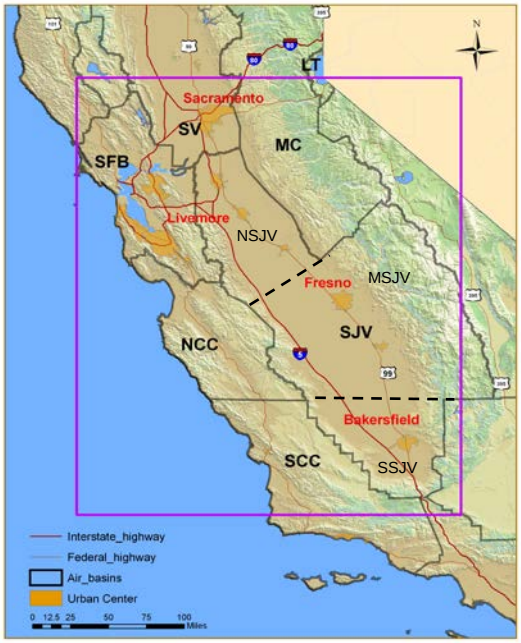

Meteorological inputs are simulated by Wilczak and co-workers at the National Oceanic and Atmospheric Administration (NOAA) (http://www.etl.noaa.gov/programs/modeling/ccos/) using the National Center for Atmospheric Research/Pennsylvania State University Mesoscale

Model (MM5) (Grell et al. 1994) version 3. A description the meteorological fields can be found in our previous work (e.g. Jin et al. 2008, 2010, 2011).

Daily emissions inputs, including gaseous and particulate species, are provided by the California Air Resources Board for months August and September of years 2000 and 2005. The emissions are not separated by source types. Biogenic emissions of methlybutanol (MBTU) are not treated explicitly, but lumped into the species class, olefin 1 (OLE1), which is also emitted anthropogenically. The emission data are first checked for quality assurance then processed with Fortran programs into gridded inputs for CMAQ simulations. Since the same meteorological inputs (year 2000) are used for the two years and variations in biogenic emissions are largely driven by light and temperature fields, the same biogenic emissions are used for the two years, and these are the biogenic emissions for year 2000. A detailed description of the emission processing is provided in Appendix A. The spatial distribution of selected gaseous emissions averaged over the two-month period is presented in Figure 2. We see that anthropogenic volatile organic compounds (AVOC) and nitrogen oxides (NO_x) are largely distributed around urban centers and highways, biogenic volatile organic compounds (BVOCs) are concentrated in mountain areas, and NH_3 is distributed throughout in the Central Valley near the major urban areas.

Figure 2: Spatial Distribution of Emissions (mol/day): Anthropogenic VOC (AVOC), NOx, Biogenic VOC (BVOC, and Ammonia (NH3)

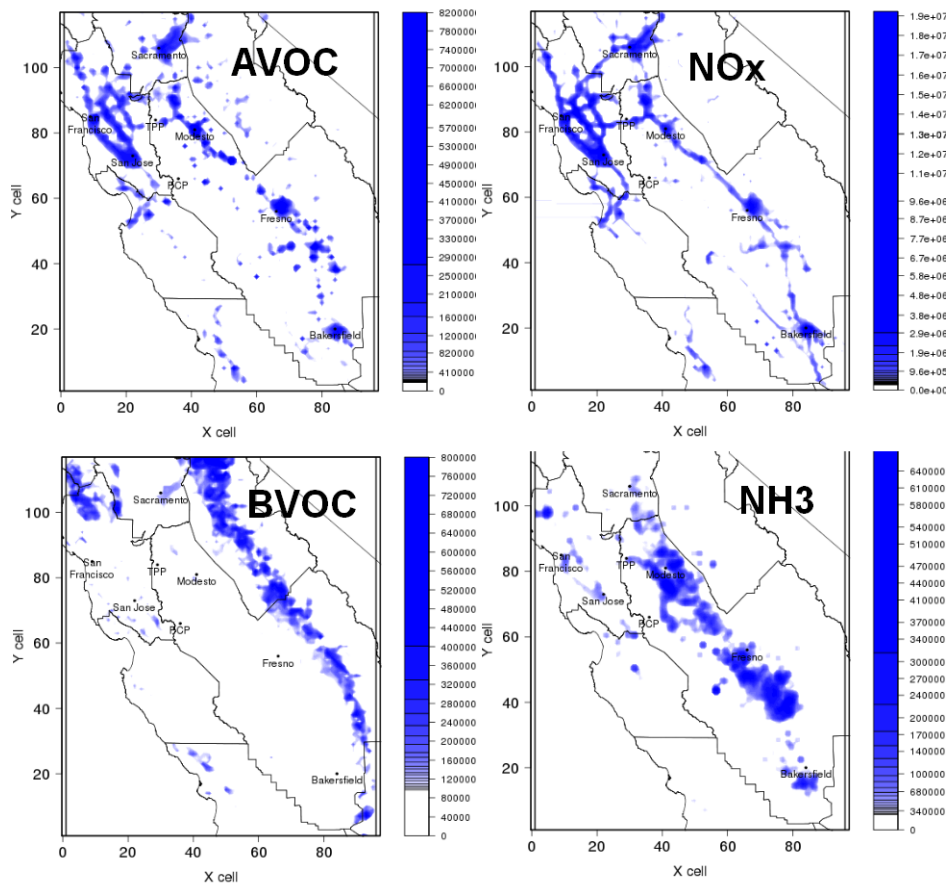

We assume constant pollutant concentrations for each of the four lateral boundaries of the modeling domain. We obtained the 2000 July boundary conditions (BCON) for the 12km x 12km California domain with 15 vertical layers used in Air Resources Board (ARB) PM modeling. The values in this BCON file are based on MOZART (version 2) output in the California domain (personal communication with Jeremy Avise at ARB). We processed the ARB boundary conditions into the 4km x 4km SARMAP domain boundary conditions with 27 vertical layers. The procedures include obtaining the four boundary vertical profiles for individual species, vertical linear interpolation of the 15 vertical layers into the SARMAP 27 vertical layers according to the pressure levels, and modifying the western and southern boundaries to reflect land/ocean differences. A detailed description of the procedures as well as a comparison to BCON values that we used in previous studies for this domain is provided in Appendix B.

CMAQv4.7.1 is configured to use the aerosol module version 5 (AERO5) and the State Air Pollution Research Center chemical mechanism produced in year 1999 (SAPRC99), and the Asymmetric Convective Model (ACM2) planetary boundary layer (PBL) scheme. The vertical layers for the CMAQ simulations match those of the meteorological simulations. Inline calculations of biogenic and plume rise emissions are not used. The base year 2000 simulations are conducted for August and September with a two-day model spinup (to eliminate any dependence on initial conditions). These simulations were used for model performance evaluation and investigation of temporal correlations between ozone and fine particulate matter.

2.2 Observational Data

Routine monitoring networks that provide long-term observations of ambient concentrations of PM (including chemical speciation) and gas-phase species include the: 1) Interagency Monitoring of Protected Visual Environments (IMPROVE) (http://vista.cira.colostate.edu/improve/); 2) Speciation Trends Network (STN, now called Chemical Speciation Network CSN); 3) Clean Air Status and Trends Network (CASTNet) (http://www.epa.gov/castnet/); and Aerometric Information Retrieval System (AIRS)-Air Quality System (AQS) (http://www.epa.gov/air/data/index.html). PM related observations include National Weather Service (NWS) visibility data (http://www.nws.noaa.gov/asos/index.html), AErosol RObotic NETwork (AERONET) (http://aeronet.gsfc.nasa.gov/), and others. The selection of species for comparison follows Appel et al. (2008).

In this study, model performance is evaluated against ambient concentration measurements of HNO_3 and fine particulate sufate (SO_4^{2-}), nitrate (NO_3^-), ammonium (NH_4^+), elemental carbon (EC), organic carbon (OC), total carbon (TC), and gravimetric mass ($PM_{2.5}$). The observed concentrations are obtained from STN, IMPROVE, CASTNet, and ARB monitoring sites.

The IMPROVE network, which began operations in 1985, with the majority of IMPROVE monitors provide 24-hour average samples for $PM_{2.5}$ mass and its components (sulfate, nitrate, organic carbon and black carbon) for every third day (midnight to midnight, local time). The

more recently established STN, developed by US EPA, follows the protocol of the IMPROVE network (i.e. every 3rd day collection) with the exception that most of the sites are found in urban areas.

Clean Air Status and Trends Network (CASTNet) evolved from US EPA's National Dry Deposition Network (NDDN) in 1990. The concentration data are collected at predominately rural sites, the majority of which are in the eastern United States, using filter packs that are exposed for 1-week intervals (i.e. Tuesday to Tuesday). It provides continuous ozone measurements and weekly samples (from Tuesday to Tuesday) for PM2.5, sulfate (SO_4), NO_3, NH_4^+, sulfur dioxide (SO_2), and HNO_3 as well as meteorological measurements over 70 sites across the United States.

The $PM_{2.5}$ mass concentrations (24-h average) are measured for areas in California to determine attainment status to the federal and state ambient air quality standards. The $PM_{2.5}$ mass is collected using the Federal Reference Method (RFM) with a low volume sampler (16.7 liters per minute) and a small (47 mm) Teflon filter for 24 hours. These 24-h average gravimetric mass measurements are used in model performance evaluation studies.

The monitoring sites that are located in our modeling domain are shown in Figure 3.

Figure 3: Monitoring Locations

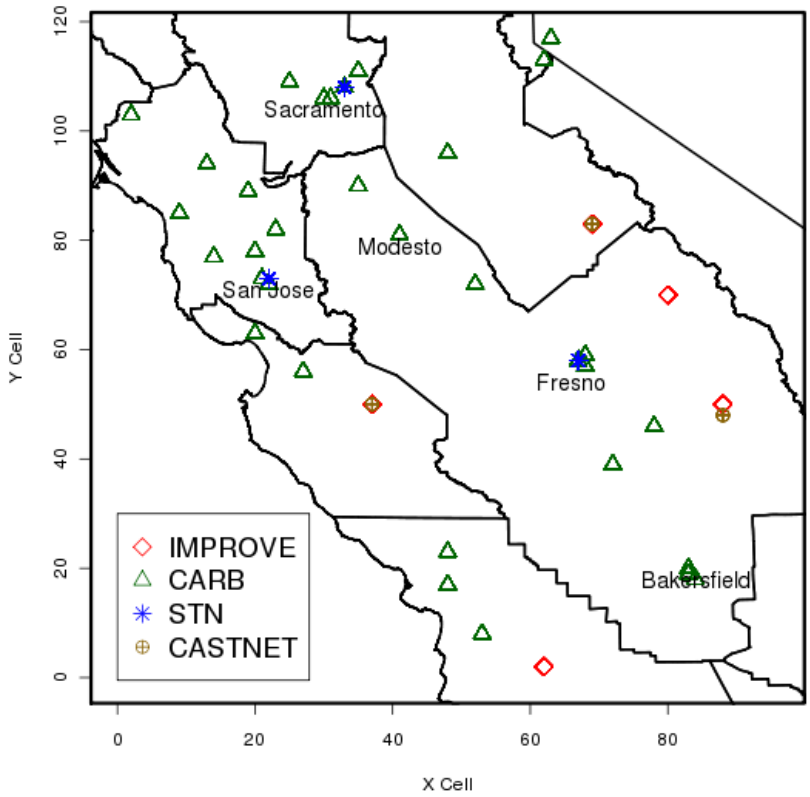

2.3 Analysis Methods

2.3.1 Paired Analysis Methods for Model Evaluation

CMAQ raw model species need to be first processed to convert into the quantities measured at various networks so that our model performance metrics can be compared to other US EPA studies. The processing protocol follows Appel et al. (2008). Fine particulate sulfate (SO_4^{2-}), ammonium (NH_4^+), nitrate (NO_3^-), and EC are approximated by summing their respective Aitken (less than 10 nm) - and accumulation-mode (less than 2.5 microns) model outputs. Fine particulate OC is estimated by following equation:

$$OC = POA*(1/1.2) + SOA_{anth}*(90/150) + SOA_{biog}*(120/177) \quad (1)$$

where POA is primary organic aerosol and SOA is secondary organic aerosol.

$PM_{2.5}$ mass is approximated by summing the modeled concentrations of all Aitken- and accumulation-mode species except water:

$$PM_{2.5} = SO_4 + NO_3 + NH_4 + POA*(1.4/1.2) + SOA_{anth} + SOA_{biog} + EC + Na + Cl + \text{Unspeciated Mass} \quad (2)$$

Statistic metrics used in paired comparison are defined in Appel et al. (2008), namely, the median bias (MdnB), the normalized median bias (NMdnB), the median error (MdnE), root mean square error (RMSE), and the normalized median error (NMdnE). Normalized quantities are given as percents.

2.3.2 Correlation Analysis

To investigate the temporal relationship between ozone and fine particulate matter (total $PM_{2.5}$ and its components), we calculated their correlations on hourly and daily time scales. Table 2 presents the quantities used in calculating the correlation coefficients. The hourly metrics used here are collocated hourly concentrations of ozone and PM species, while the daily metrics are 8-h daily maximum ozone and 24-h average PM species. These daily metrics are chosen because they are closely related to the National Air Quality Standards regulated by US EPA.

Table 2: Quantities for Calculating Temporal Correlations of Daily and Hourly Time Scales

	Daily Metric	Hourly Metric
O_3	Daily 8h maxima	Hourly
PM species	24h average	Hourly

The Pearson correlation coefficients (cor) are calculated between two variables X and Y as follows:

$$r = \frac{\sum_{i=1}^{n}(X_i - X)(Y_i - Y)}{\sqrt{\sum_{i=1}^{n}(X_i - \bar{X})^2}\sqrt{\sum_{i=1}^{n}(Y_i - \bar{Y})^2}} \tag{3}$$

Where i is the time index, and n is the sample number.

The partial correlation coefficients (pcor) between X and Y, when the effects of a set of controlling variables Z are removed, are calculated as follows:

1.Regress x and y on z separately to get estimated $\hat{x}$ and $\hat{y}$:

$$x = \alpha \cdot z + \varepsilon \rightarrow \hat{x} = \hat{\alpha} \cdot z$$
$$y = \beta \cdot z + \varepsilon \rightarrow \hat{y} = \hat{\beta} \cdot z$$

2. Calculate

$$pcor(x, y) = cor(x - \hat{x}, y - \hat{y})$$
$$= cor\left(x - \hat{\alpha} \cdot z\ , y - \hat{\beta} \cdot z\ \right)$$

The controlling variables are meteorological quantities of temperature, relative humidity, PBL height, and wind speed.

2.3.3 Sensitivity Analysis

Due to computational costs, the sensitivity simulations are conducted for two episodes that have different meteorological conditions: August (Julian days 227-230) and in September (Julian days 261-264) of year 2000 and 2005.

Figure 4: Afternoon Sea Surface Pressure (100 Pa) and Temperature (K) Anomalies (Relative to the Seasonal Mean) Averaged over the Two Episodes

The purple arrows indicate wind flow induced by the sea surface pressure gradients.

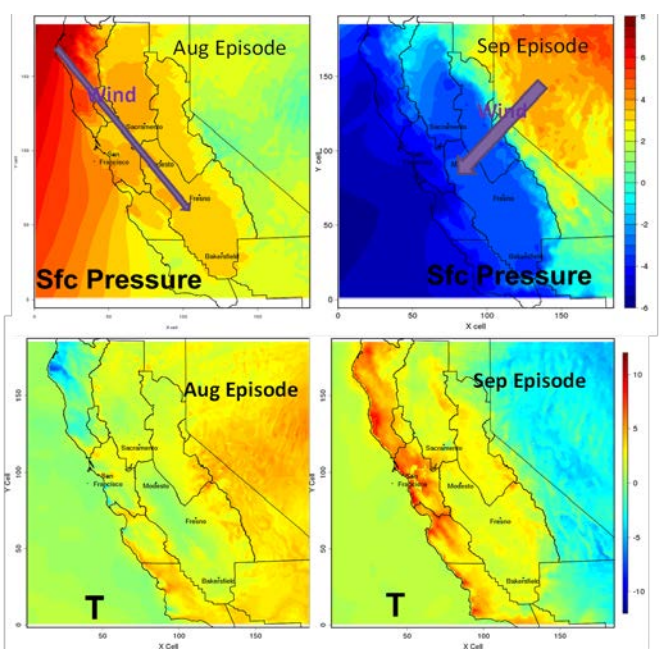

The temperature and sea level pressure anomalies are presented in Figure 4 to illustrate the meteorological differences between the two episodes, which are also summarized in Table 3.

Table 3: Meteorological Conditions of the Two Episodes

	Temperature	RH	Stagnation	Wind Flow
Aug Episode (Aug 14th to 17th)	Higher inland	About the same	Ventilated	On-shore
Sep Episode (Sep 17th to 20th)	Higher coastal	About the same	Very stagnant	Off-shore

First order (S_p^1) and second order (S_p^2) semi-normalized sensitivity coefficients of concentration C to parameter p are approximated by brute force perturbations:

$$S_p^1 = \frac{\partial C}{\partial \varepsilon_p} \approx \frac{C_{p+10percent} - C_{p-10percent}}{0.2} \tag{4}$$

$$S_p^2 = \frac{\partial^2 C}{\partial \varepsilon^2} \approx \frac{C_{p+10percent} + C_{p-10percent} - 2 \cdot C_p}{0.1 \cdot 0.1} \tag{5}$$

$\boldsymbol{\varepsilon}_p$ is the fractional perturbation of parameter p. C_p, $C_{p+10\%}$, *and* $C_{p\ -10\%}$ are Concentrations evaluated at base the case with parameter p and for cases where p is perturbed by +10percent and -10percent, respectively. The approximations for the first order sensitivities (S_p^1) and the second order (S_p^2) semi-normalized sensitivity coefficients are derived from the Taylor theorem:

$C = C_0 + \boldsymbol{\varepsilon}_p \cdot S_p^1 + 0.5\boldsymbol{\varepsilon}_p^2 \cdot S_p^2 + \text{HOT}$, where HOT is higher order terms (~ $O(\boldsymbol{\varepsilon}_p^3)$).

CHAPTER 3:
Base Year Simulations and Model Performance

3.1 Spatial and Temporal Distribution of Simulated Ozone and $PM_{2.5}$

CMAQ simulations are conducted for the August and September periods of year 2000. The average spatial distributions of daily maximum 8-h ozone and 24-h average $PM_{2.5}$ are presented in Figure 5. Higher maximum 8-h average ozone levels (>60 ppb) are located in the middle and southern parts of the SJV, and these are of large spatial extent. On the contrary, high average $PM_{2.5}$ (>15ug/m3) are located in a narrow central corridor of the SJV, largely in the vicinity of NH_3 emissions (see Figure 1). The spatial gradients of $PM_{2.5}$ are much sharper than ozone.

Figure 5: Period Averages for (a) Maximum 8 h Average O_3, (b) 24 h Average $PM_{2.5}$, (c) Log of Adjusted Gas Ratio (AdjGR)

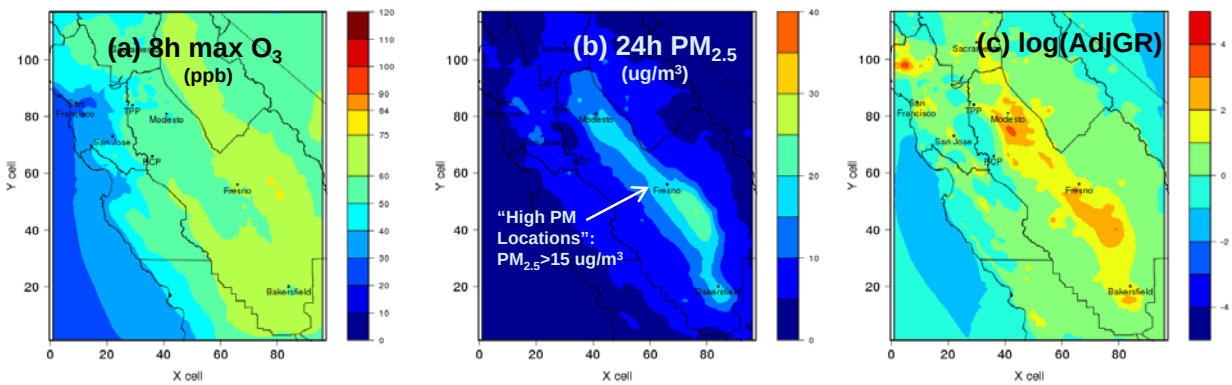

Adjusted Gas Ratio (Pinder et al. 2008), AdjGR, is evaluated by calculating the ratio: $([NH_3]+[NO_3])/([HNO_3]+[NO_3])$. AdjGR indicates whether NH_4NO_3 formation is limited by NH_3. AdjGR>1 or log(AdjGR)>0 generally indicates NH_3 is in excess and that there is a deficiency of HNO_3. Figure 5(c) indicates that the NH_4NO_3 formation is most likely to be limited by HNO_3, because NH_3 is abundant in the valley, especially for the locations with high PM (>15ug/m^3).

The diurnal profiles of $PM_{2.5}$, ozone, and gaseous HNO_3 concentrations are averaged for the location having high PM (>15 ug/m^3), and are shown in Figure 6. Among the secondary aerosols, nitrates, on average, dominate the $PM_{2.5}$ mass and determine its diurnal cycle at "high PM locations". Higher NH_4NO_3 is observed at night and early morning while lower NH_4NO_3 occurs during the photochemically active hours. As indicated by the ozone and HNO_3 diurnal profiles, the availability of oxidants and HNO_3 are highest during the photochemically active hours. Therefore, lower particulate NH_4NO_3 during these high HNO_3 hours are more likely to be regulated by high temperatures that limit the gas-to-particle conversion. Particulate sulfates are low and not variable, which indicates a lack of precursor emissions and small production rates at these locations.

Figure 6: Diurnal Profiles of $PM_{2.5}$, Components, O_3 and Gaseous HNO_3 Averaged over Locations with $PM_{2.5}$ >15 ug/m^3 in Figure 5

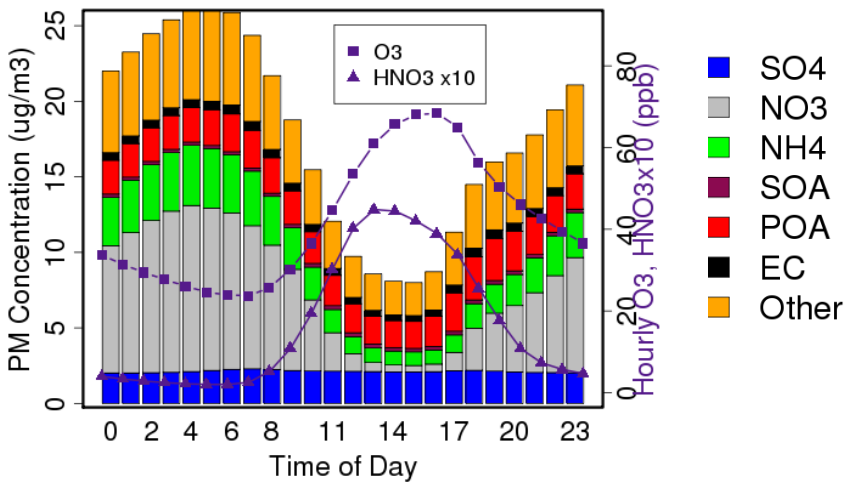

3.2 Paired Performance Metrics

Performance statistics are calculated for RMSE, median bias (MdnB), normalized median bias (NMdnB), median error (MdnE), and normalized median error (NMdnE) with respect to modeled vs observed PM species at the four monitoring network locations. Normalized quantities are given as percents.

Total $PM_{2.5}$ mass shows a small negative bias at remote locations (IMPROVE) sites, and positive biases at urban locations (STN and ARB). Model performance at the IMPROVE and STN sites is consistent with findings from Appel et al. (2008) on CMAQ performance in the eastern US with urban biases systematically higher than the rural predictions. At ARB sites, CMAQ overpredicts the higher $PM_{2.5}$ masses, which generally occur in September. This behavior was also observed in Appel et al. (2008). The ARB samples are collected using Teflon filters. Total $PM_{2.5}$ mass is collected on Teflon filters, which are known to have negative biases for the semi-volatile components under higher temperature conditions (Chow et al. 2006) due to evaporative losses. This issue can be especially important in the SJV where particulate nitrates dominate the secondary inorganic $PM_{2.5}$.

Comparison of simulation results with measured values at all the networks (rural and urban) shown in Figure 7 indicate that particulate nitrates (by about - 0.16 to - 0.3 ug/m^3) are underpredicted and particulate sulfates (by about 0.15 to 0.44 ug/m^3) are overpredicted as is NH_4 (by about 0.23 to 0.38 ug/m^3). As indicated earlier, the inorganic aerosol chemistry is not limited by the availability of ammonia; hence, the impact of errors in ammonia emissions on particulate nitrates and sulfates should be small. This is different from the eastern US, where a large source of error in predicting aerosol NO_3 mass stems from errors in predicted NHx (NH_3+NH_4^+) and SO_4. However, an overprediction of particulate SO_4^{2-} is a result of overestimation of sulfur oxide (SOx) emissions. Additionally, boundary conditions can potentially lead to overprediction of total particulate NH_4^+ especially at remote sites where

NH_4NO_3 is less dominant. At remote sites (CASTNet), the total NO_3 (TNO_3=HNO_3+particulate NO_3) and HNO_3 concentrations are overpredicted, which is consistent with findings discussed in Appel et al. (2008) for the eastern US; however, the cause of this overprediction is not understood.

Carbonaceous aerosols (EC, OC, and TC) are underpredicted by the model as shown in Figure 7. The TC predictions are poorer at urban sites (STN) (bias = -2 ug/m^3) than at the remote sites (IMPROVE) (bias = -0.4 ug/m^3). Previous CMAQ simulations (e.g. Tesche et al. 2006) found EC and OC were underpredicted throughout the year with the largest underpredictions occurring in the summer and fall. Underestimates of primary EC emissions and secondary organic aerosol (SOA) formation were identified as potential causes for this in previous model performance evaluations.

Figure 7: Modeled vs Observed PM Species at the Four Monitoring Network Locations.

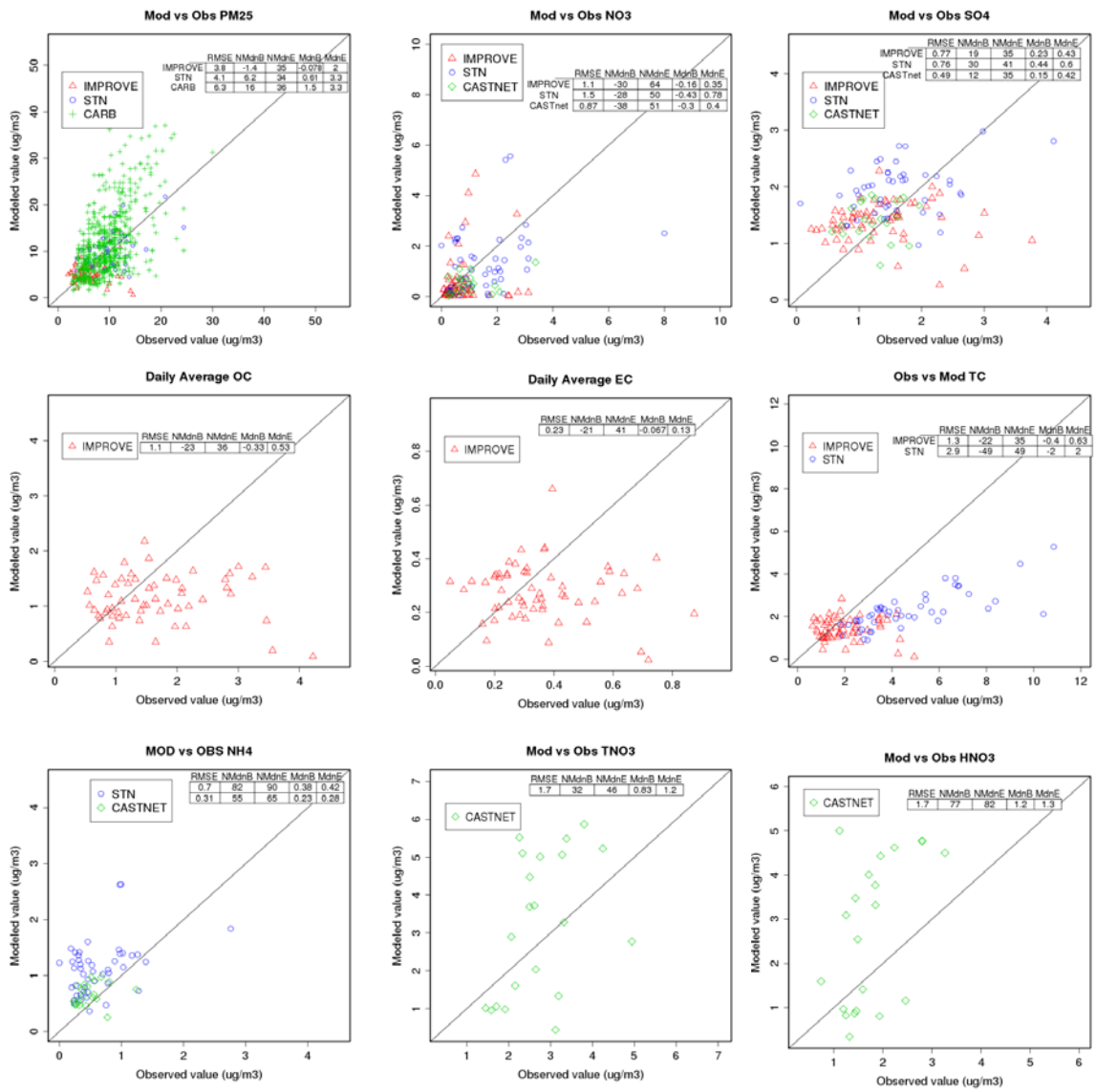

3.3 Modeled vs Observed PM Composition

Stacked bar charts showing $PM_{2.5}$ composition are averaged over modeling periods commensurate with the sampling period used for IMPROVE sites (aggregated to Coastal sites and Sierra sites to improve sample sizes) and STN sites (Figures 8 and 9). In urban sites, the most noticeable difference in $PM_{2.5}$ compositions between model and observational results is in the total carbonaceous aerosols, followed by SO_4 and NH_4^+ aerosols. The model underpredicts TC at urban sites and overpredicts particulate SO_4 and NH_4. In remote locations, the model underpredicts OC in Sierra sites where biogenic emissions are dominant and SOA formation is potentially more important but is not captured well by the model. EC is underpredicted at Sierra sites, indicating that the primary emissions are underestimated. This is also true for other primary OC. Modeled compositions at the coastal sites achieve better agreement with observational values than those at Sierra sites. This disagreement does not mean that the model is bad, but rather speaks to the difficulty in comparing modeling results of PM with measured values since measured values are frequently collected and measured differently in different networks. Sample integrity is often a problem as well. The science associated with PM is not nearly as refined as that associated with ozone.

Figure 8: Modeled vs Observed $PM_{2.5}$ Composition at IMPROVE Sites (Remote).

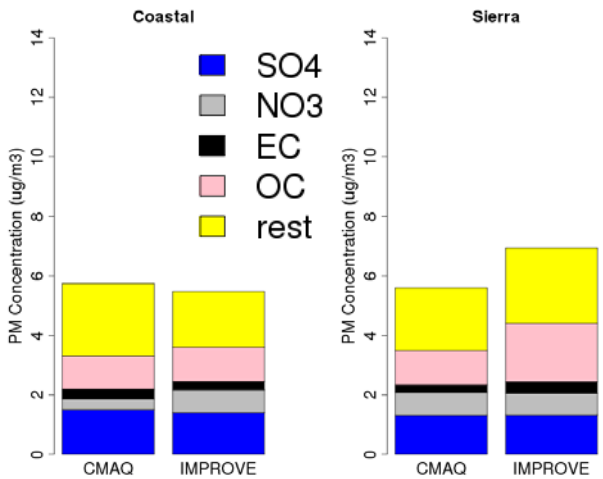

Figure 9: Modeled vs Observed $PM_{2.5}$ Composition at STN Sites (Urban).

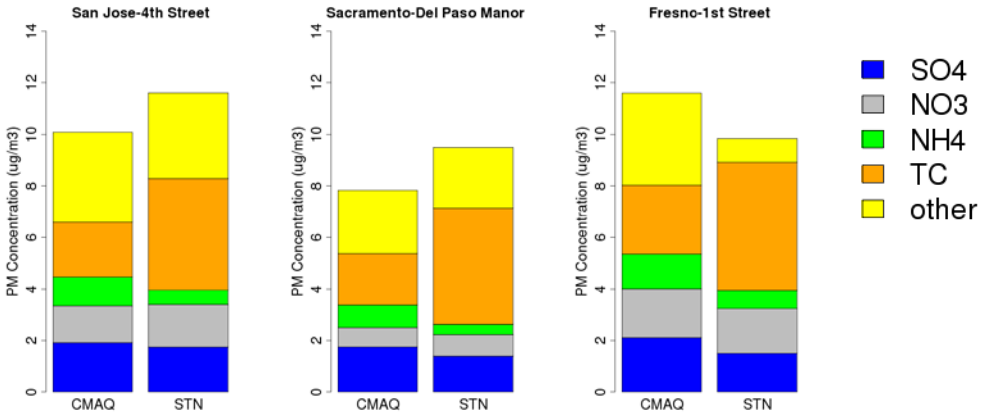

CHAPTER 4:
Temporal Relationship between Ozone and $PM_{2.5}$

4.1 Pearson Correlation

Pearson correlation coefficients, as an indicator of the association between ozone mixing ratios and $PM_{2.5}$ mass concentrations over the two-month period of year 2000, are calculated using hourly and daily metrics defined in Chapter 2. The analysis focuses on "high PM" locations defined in Figure 5 (b). Pearson correlation coefficients over the "high PM" grid cells are summarized with histograms in Figure 10.

Figure 10: Statistical Distribution of Hourly and Daily Correlation Coefficients between Ozone and $PM_{2.5}$

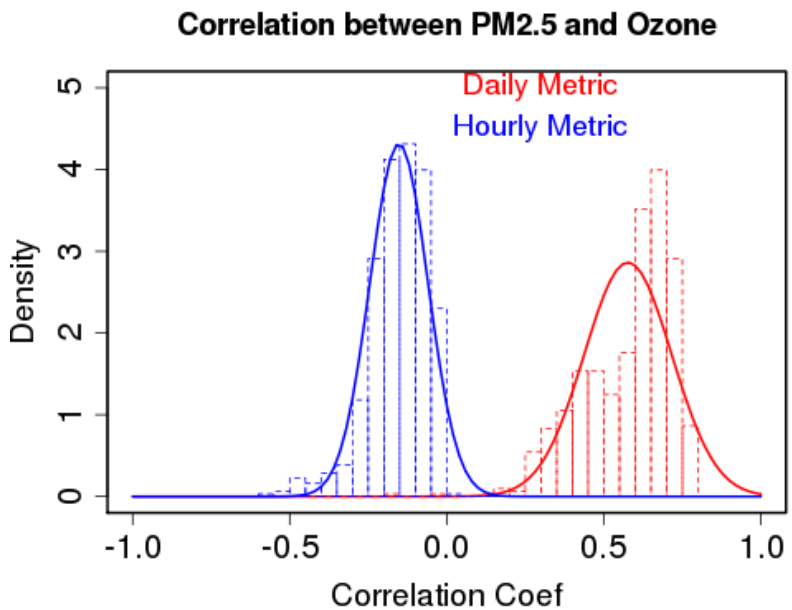

On the hourly time scale, $PM_{2.5}$ and ozone are negatively correlated rather weakly (with most correlation coefficient absolute values < 0.3). In contrast, on the daily time scale, $PM_{2.5}$ and ozone are positively and strongly correlated (with most correlation coefficients > 0.5). The correlation between total $PM_{2.5}$ mass and ozone is determined by the temporal behavior of individual $PM_{2.5}$ components. According to Figure 6, the major contributors to $PM_{2.5}$ mass over the high PM locations are particulate SO_4, NO_3, NH_4^+, POA, and PM_{other}. Temporal correlations between these individual components and ozone at hourly and daily time scales are evaluated and summarized in Figure 11.

Figure 11: Statistical Distribution of Hourly and Daily Correlation Coefficients between Ozone and $PM_{2.5}$ Species

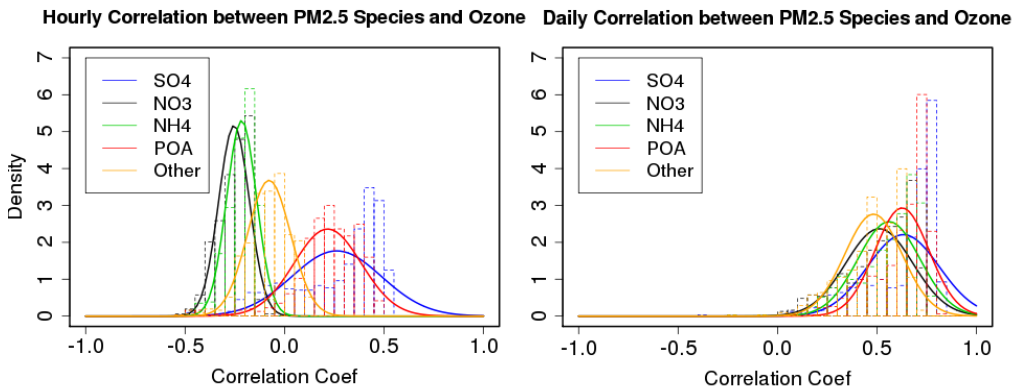

Examination of Figure 11 indicates that on hourly time scales, the signs of correlation between $PM_{2.5}$ components and ozone are mixed. Ammonium nitrate (NH_4NO_3) (designated as NO3 and NH_4^+ in the figure) hourly variations are negatively correlated with ozone, while thermally stable components e.g. POA and particulate sulfates largely showed positive correlations with hourly ozone. PM_{other} consists of trace elements and other unidentified mass in the primary emissions, and its correlation with ozone does not have a consistent sign As seen in Figure 6, nitrates, on average, dominate the $PM_{2.5}$ mass and drive its diurnal cycle at "high PM locations". The negative correlation presented in Figure 10 between hourly total $PM_{2.5}$ mass and ozone is largely driven by the negative correlation between hourly NH_4NO_3 and ozone. In contrast, all the $PM_{2.5}$ components show positive correlations with ozone on the daily time scale (Figure 11 right), which explains the stronger positive correlation between PM mass and ozone.

4.2 Partial Correlation

The positive correlations between the daily metrics indicate that higher 8-h max ozone and 24-h average $PM_{2.5}$ tend to occur together. The different signs of hourly and daily correlations of ozone with $PM_{2.5}$ can be explained by their dependence on meteorological variables. Figure 12 illustrates a conceptual framework of meteorological effects on nitrates and ozone. We focus on nitrate instead of $PM_{2.5}$ because, as discussed earlier, the different signs of hourly and daily correlation coefficients of ozone with $PM_{2.5}$ are largely determined by the correlation between nitrate and ozone.

PBL height and wind speed affect ozone and $PM_{2.5}$ similarly through their influence on the physical transport of pollutants (e.g. dilution, advection). Temperature and relative humidity (RH) exert opposite effects on ozone and nitrate. Higher temperature is found to be associated with higher ozone (Weaver et al. 2009 and references therein). Higher RH is inversely related to absolute humidity in central California's dry summer season, because variations in RH are controlled by temperature. Lower RH is associated with higher values of absolute humidity, which in turn, favors production of [OH] radicals and promotes ozone formation. In contrast, lower RH and higher temperatures cause evaporation of particulate nitrates and reduce their concentration (Lunden et al. 2006). Besides the meteorological factors, ozone and nitrate are

positively associated because of the NO oxidation chemistry that forms HNO_3. Such relationships are revealed only after the meteorological effects are removed.

Figure 12: Conceptual Framework of Potential Meteorological Effects on Nitrates and Ozone

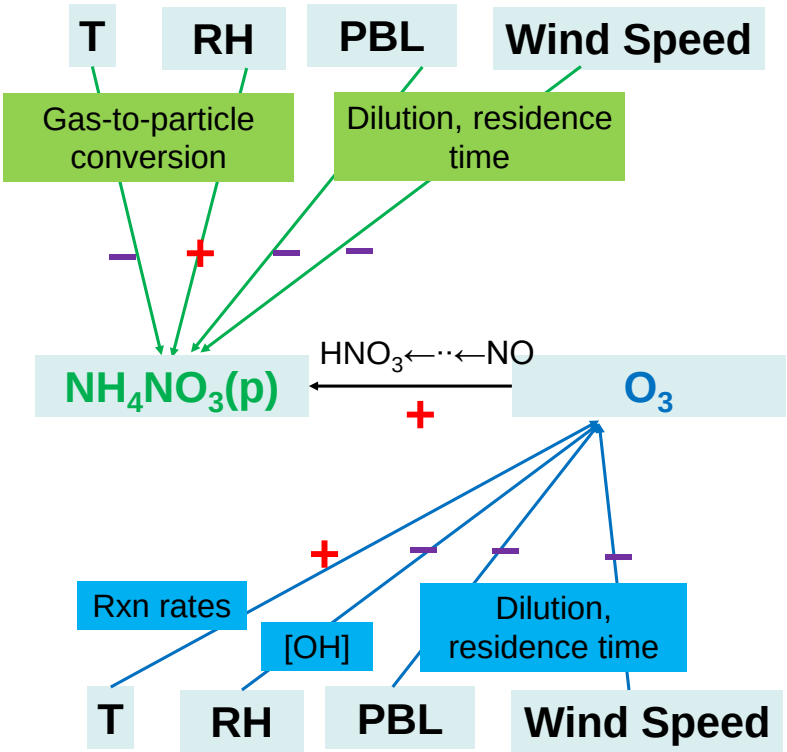

Figure 13: Partial Correlation Coefficients between O_3, PM, and Meteorological Variables on Hourly (upper) and Daily (Lower) Timescales

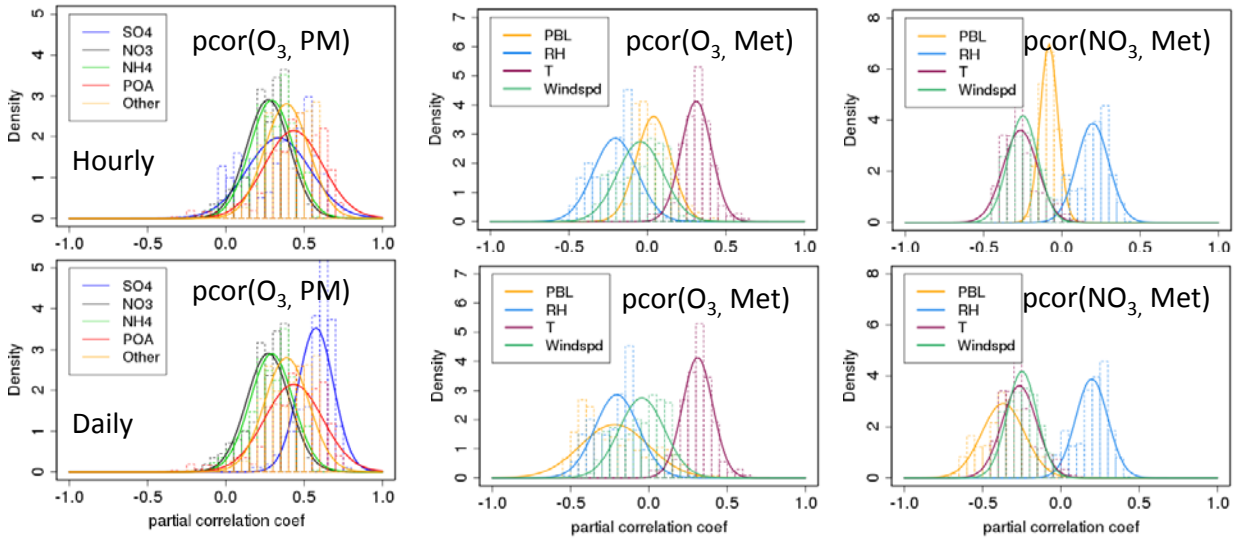

Figure 13 shows the partial correlation between ozone and $PM_{2.5}$ species after the meteorological effects are removed by linear regression (see Chapter 2 for descriptions). The negative hourly correlations between NH_4NO_3 and ozone, as noted previously are now positive, as illustrated in Figure 12. Partial correlations between pollutants and meteorological variables are also shown in Figure 13 for hourly and daily timescales. On both timescales, temperature and RH have partial correlations with ozone and nitrates of opposite signs, which confirms the conceptual model illustrated in Figure 12. However, effects of PBL and wind speed on ozone and nitrate behave differently on hourly and daily timescales. On the hourly timescale, PBL and wind speed do not have the consistent partial correlations with ozone that they have with nitrates. Overall meteorological effects considered here are dominated by the temperature and RH effects, which are opposite for ozone and nitrates, and contribute to the overall negative correlation between ozone and $PM_{2.5}$. On the daily timescale, despite the fact that the wind speed partial correlation with ozone and nitrates does not have consistent signs, the PBL has negative partial correlations with both pollutants. Lower PBL values indicate stagnant conditions. The common negative partial correlations between PBL and ozone/nitrates indicate that stagnant conditions can potentially induce both higher nitrate and ozone on daily timescales. The PBL effects reinforce the positive partial correlations between ozone and nitrates on daily timescales and contribute to the overall positive correlation between $PM_{2.5}$ and ozone.

CHAPTER 5:
Ozone and $PM_{2.5}$ Responses to Emission Controls

From previous chapters we have seen that high ozone (8h maxima) and $PM_{2.5}$ (24h daily average) tend to occur together during the late summer and early fall time (August and September) under more stagnant conditions (indicated by lower PBL heights). Hence, it is important to consider control of these two pollutants in concert. NH_4NO_3(p) dominates the $PM_{2.5}$ mass and drives its temporal variations (especially diurnal) at high PM locations (i.e. August-September average 24h $PM_{2.5}$ > 15 ug/m^3). The formation of NH_4NO_3(p) is generally limited by HNO_3(g) (Figure 5) in regions where PM is high.

HNO_3 (g) formation is coupled to ozone chemistry by sharing the same precursors (NO_x and AVOCs) as shown below.

- Daytime: photochemistry VOC + NO_x+… → OH+NO_2+M→HNO_3→gas to particle phase conversion (regulated by T, RH etc..)
- Nighttime: O_3+NO→ NO_2+NO_3+M→heterogeneous chemistry→ N_2O_5+H_2O(s)→HNO_3

Here chemical coupling is defined as responses of ozone and PM to common precursors. When coupling is strong and positive, there are potential opportunities to control both pollutants together.

Meteorology influences ozone sensitivities to its precursors, and it may change the chemical coupling between ozone and PM nitrate. The research questions addressed in this chapter are:

1. How do ozone, $PM_{2.5}$ and their sensitivities to VOC and NO_x vary with meteorology?
2. Does the meteorological dependence on the chemical coupling change with emissions?
3. Can precursor (AVOC or NO_x) controls benefit both pollutants?

Two selected episodes (August and September episodes, see Chapter 2 for descriptions) are used for conducting the sensitivity simulations. In addition to year 2000 emissions, emissions from a more recent year (year 2005) are used. Sensitivity analysis is focused on year 2005.

5.1 Meteorological Effects on Concentrations and Chemical Coupling

Episodic averages of 24-h $PM_{2.5}$ mass and 8-h ozone maxima of year 2005 are presented in Figure 14. Both ozone and PM concentrations are higher in the more stagnant September Episode consistent with findings in the previous chapter. The 8-h maximum ozone levels exceeding the current 75 ppb standard are located in the middle and southern parts of the SJV, while exceedances over 60 ppb are much more extensive throughout the valley for the September episode.

Figure 14: Episode Averaged 8h Ozone Maxima (Left) and 24h Average $PM_{2.5}$ (Right) for August (Upper) and Sep (Lower) Episodes for Year 2005

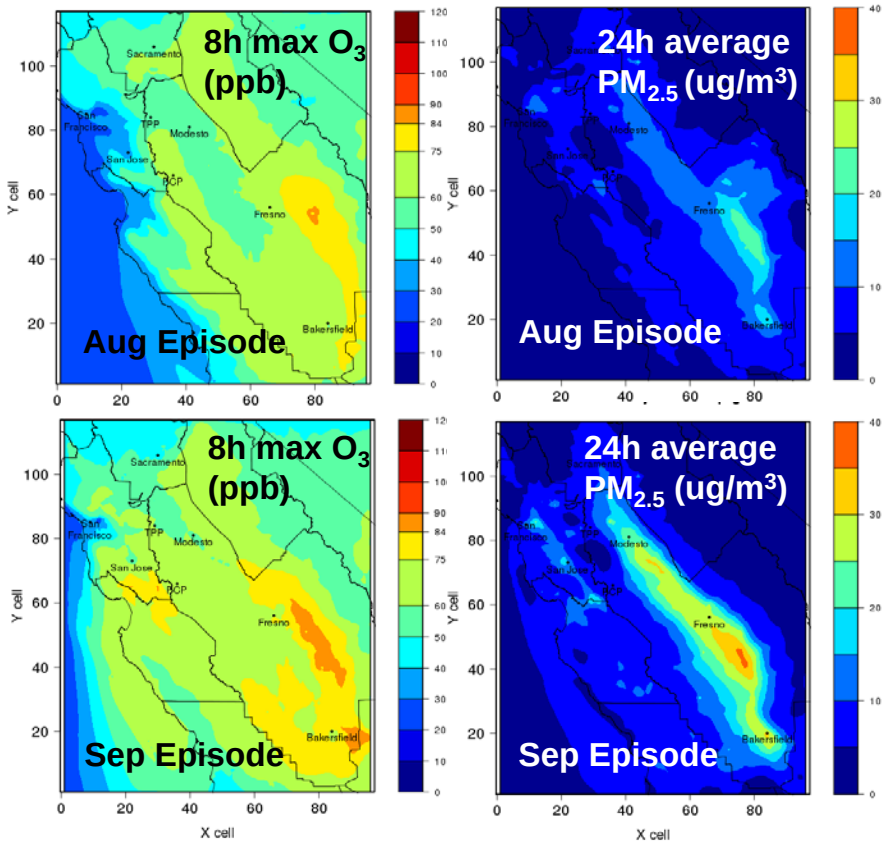

First-order semi-normalized sensitivities are calculated for both ozone and $PM_{2.5}$ with respect to their common precursors NOx and AVOC. The episodic averages are presented in Figure 15. Ozone response to NOx emissions is highly nonlinear as indicated by the negative sensitivities (NOx disbenefit) in high NOx areas, while ozone responses to AVOC are always positive. The NOx disbenefit to ozone is greater in magnitude (deeper blue color in Figure 15) in the September episode due to greater stagnation and it is more spatially extensive in the August episode due to the increased southeastward transport. $PM_{2.5}$ sensitivities to NOx also have higher magnitudes in the more stagnant September episode. While ozone is both sensitive to NOx and AVOC, $PM_{2.5}$ shows very small negative sensitivities to AVOC (not shown in Figure 15, but can be seen in Figure 16).

Figure 15: Episode Averaged Semi-Normalized First Order Sensitivity of 8h Ozone Maxima to AVOC and NO_x Emissions and S^1 Sensitivities of 24h Average $PM_{2.5}$ to NOx Emissions for August (Upper) and September (Lower) Episodes in Year 2005

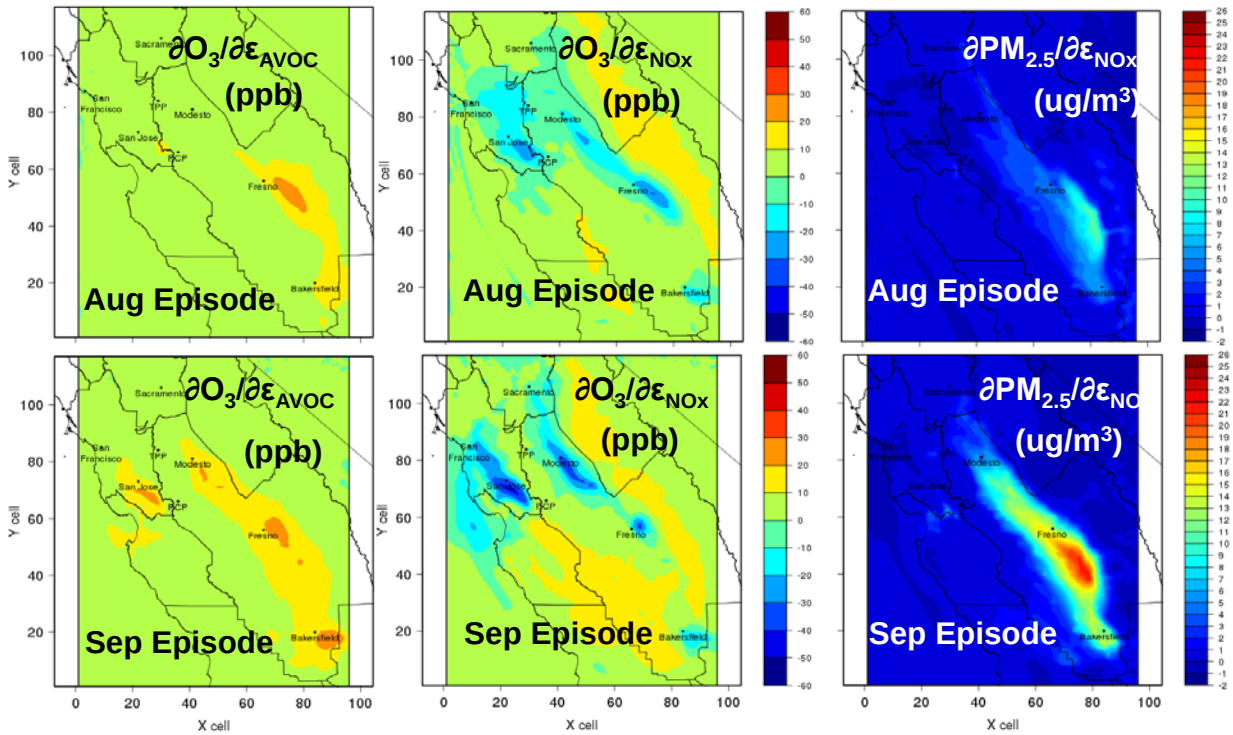

The hourly sensitivities of $PM_{2.5}$ are decomposed further into the individual PM components and averaged over the "high PM" locations (Figure 16). High PM locations are defined similarly as in the previous chapter where late-summer-early-fall (August-September) average 24-h $PM_{2.5}$ levels are greater than 15ug/m^3. The $PM_{2.5}$ sensitivities to NOx are dominated by sensitivities of NH_4NO_3 to NOx, reflecting that HNO_3 formation (24h average) is NO_x limited. The sensitivities of NH_4NO_3 to NOx are high during morning and nighttime, and are higher in the more stagnant September episode. Figure 16 indicates that the ammonium pernitrate (NH_4NO_4) formation chemistry, on average, is limited by NOx while ozone chemistry is limited by AVOC (NO_x disbenefit) for the high PM locations. Although $PM_{2.5}$ and ozone both showed an increase in the magnitude of pollutant sensitivities to precursor emissions under the more stagnant conditions, their limiting precursors are, on average, different at the "high PM" locations. Targeting the reduction of PM nitrates can be achieved more efficiently by reducing NO_x, which would result in an increase in ozone concentrations. In light of new potentially more stringent ozone regulations, this would be most unfortunate.

Figure 16: Hourly O_3 and $PM_{2.5}$ Sensitivities to AVOC (Left) and NOx (Right) Averaged for August (Upper) and September (Lower) Episodes of Year 2005 at "High PM Locations". The PM Sensitivities are Further Decomposed into Sensitivities of PM Components to AVOC and NO_x.

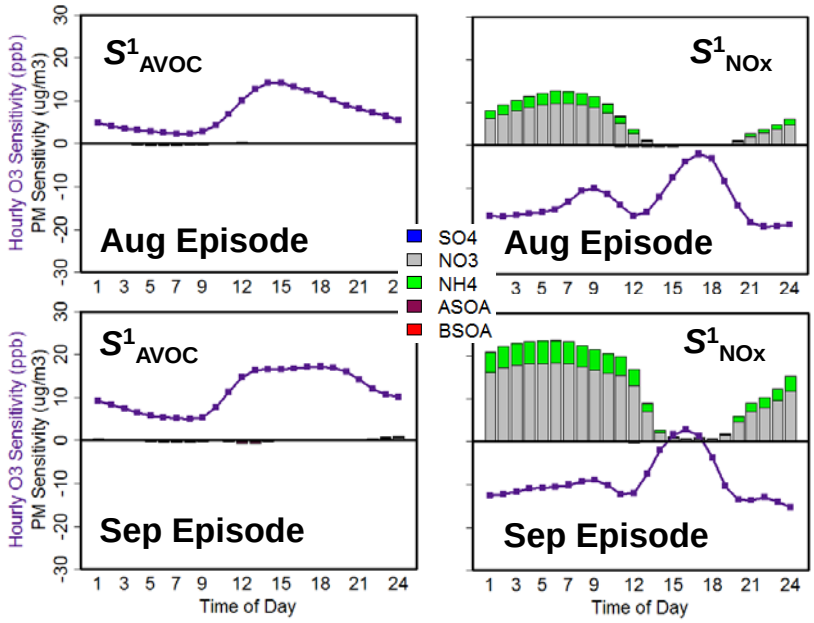

Other precursor emissions to secondary PM are NH_3 and SO_x. First-order semi-normalized sensitivity coefficients of $PM_{2.5}$ to these precursor species are also calculated and plotted for the "high PM" locations for the two episodes (Figure 17). Controlling NH_3 or SO_x can achieve lower $PM_{2.5}$ but this is not as effective as controlling NOx according to the magnitude of the semi-normalized sensitivity coefficients. Reducing NH_3 emissions decreases $PM_{2.5}$ through a decrease in the formation of particulate NH_3NO_3. Reducing SOx emissions not only decreases particulate sulfates but also particulate nitrates due to changes in the ionic strength that occurs with reduced particle-bound water.

Figure 17: Hourly $PM_{2.5}$ Sensitivities to Ammonia (Upper) and SOx (Lower) Emissions Averaged for August (Left) and September (Right) Episodes of Year 2005 at "High PM Locations". The PM Sensitivities are Further Decomposed into PM Components with Same Legend as in Figure 16

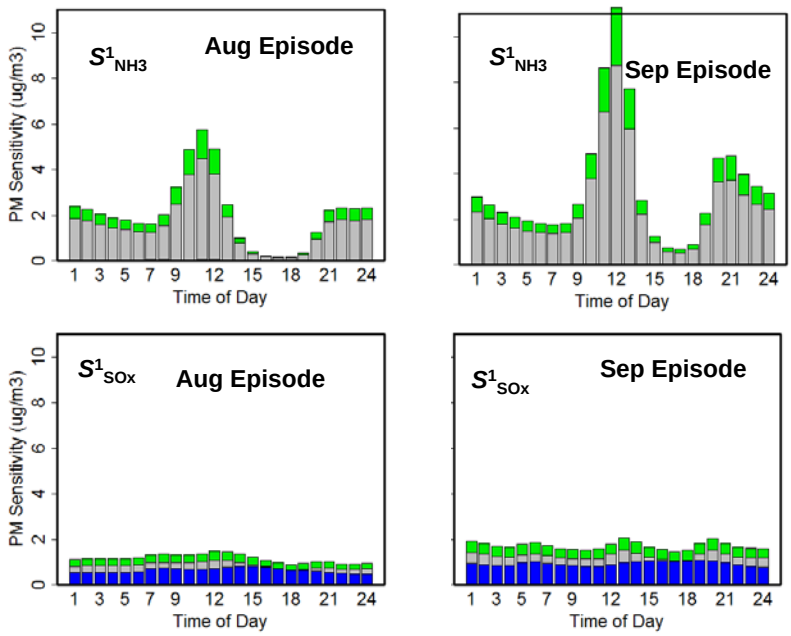

5.2 Meteorology vs Emission Effects on Ozone

As seen earlier, NOx control that benefits $PM_{2.5}$ would, on average, result in an increase of 8-h ozone maxima at the high PM locations, which complicates the control of the two pollutants together. Due to the non-linearity of the ozone chemistry with respect to NO_x emissions, this analysis focuses on the interaction of ozone and its sensitivities with meteorology and emissions.

Both meteorology and emission variations can affect pollutants concentrations and their sensitivities. AVOC and NOx emissions have been reduced from year 2000 to 2005 by more than 10percent (Table 4). Figure 18 compares the distribution of ozone levels at the high PM locations over the two episodes between the two years. Ozone levels in the August episode are lower than the September episode, only ~10percent exceed the current 75 ppb standard. However, the changes in ozone with the emission reductions that occurred from 2000 to 2005 are smaller under the meteorological conditions in August than in September (i.e. the light and dark blue lines are further apart than the light and dark red lines). Such behavior indicates that the stagnant episode with higher pollutant concentrations also experiences greater reductions of ozone levels than the cleaner (more ventilated) episodes with the same emission reductions.

Table 4: Common Precursor Emissions (Averaged over Mondays)

Tons/day	AVOC*	NOx*
Year 2000	1400	1500
Year 2005	1250	1300

Figure 18: Cumulative Distribution of 8h Max O_3 over High PM Locations. Vertical Lines Correspond to 60 ppb (Possible Future O_3 Standard), and 75 ppb (Current O_3 Standard)

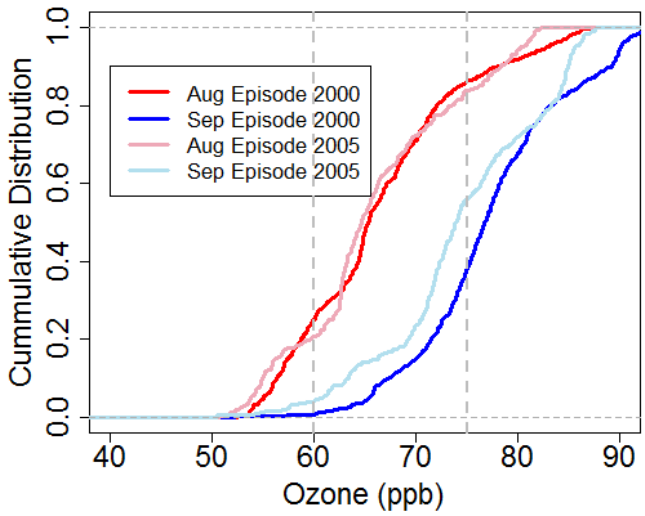

Figure 19 summarizes first-order ozone sensitivities to NOx in the two episodes for the two years at high PM locations. The sensitivities are spatially disaggregated by different levels of 8-h max ozone. The distribution of ozone to NOx sensitivities tends to shift positively with emission reductions that occurred from 2000 to 2005, especially for the NOx disbenefit areas in September. Ozone sensitivity with emissions changes in the August episode are small. Higher ozone (>75 ppb) tends to collocate with higher PM in NOx rich locations/urban ($S^1_{NOx}<0$) in August and in NOx poor/rural areas ($S^1_{NOx}>0$) in September because higher PM can be built up in rural locations under more stagnant conditions. Under the stagnant conditions, NOx control can benefit both ozone and $PM_{2.5}$ where ozone (>75 ppb) and $PM_{2.5}$ (>15 ug/m^3) are both high. As emissions are reduced from year 2000 to year 2005, the middle range ozone (60~75 ppb) also begins to reveal positive sensitivity to NOx; a transition occurs, and NOx control becomes beneficial to both pollutants under the stagnant conditions. However, under the more ventilated conditions, the NOx disbenefit to ozone is observed through all the ozone levels for both years.

Figure 19: Distribution of O_3 to NO_x Sensitivities over High PM Locations for Different Ozone Levels. The Median (Horizontal Line) in Each Box Indicates a Central Tendency of the Distribution

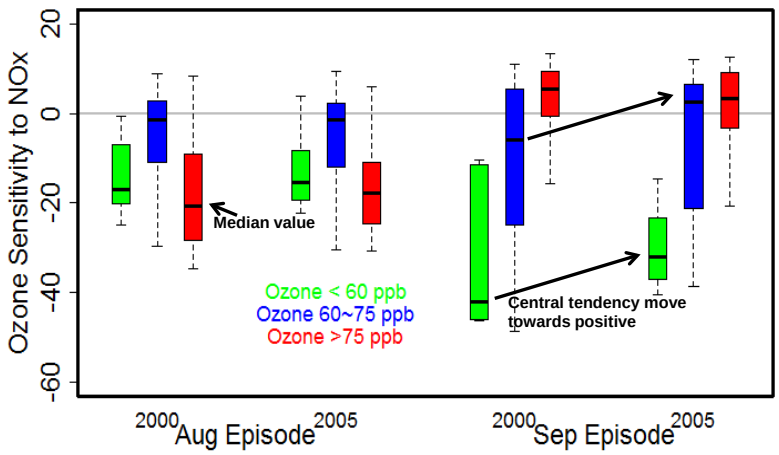

Ozone changes with further reduction of NOx emissions are approximated by a Taylor Expansion. We calculate new ozone levels with ε representing the fraction of NOx reduction that has occurred using the first- and second-order ozone sensitivities to NOx as follows:

$$O_3 \mid_{(1-\varepsilon)NOx} = O_3 - \varepsilon \cdot S^1_{NOx} + 0.5 \cdot \varepsilon^2 \cdot S^2_{NOx} \qquad (6)$$

The average 8-h ozone maxima over high PM locations as a function of percentage NOx reduction from year 2005 level are presented in Figure 20. We can see that NOx control becomes beneficial for both ozone (averaged over all the ozone levels) and PM when larger amount of NOx are reduced an additional 15 percent for the September met conditions, and an additional 30 percent for the August meteorological conditions.

Figure 20: Average 8h Max O_3 over High PM Locations with Reduction (Percent) of NO_x of Year 2005 Level

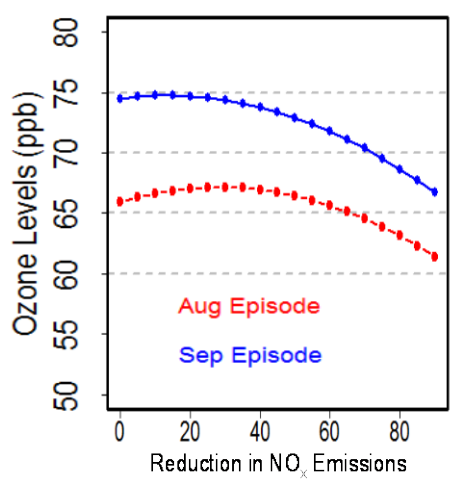

CHAPTER 6: Conclusions

Particulate matter and ozone controls are traditionally considered separately because their high pollution periods are not concurrent on seasonal timescales. California's San Joaquin Valley is out of compliance with both $PM_{2.5}$ and ozone standards. Ozone concentrations are high in the summer and $PM_{2.5}$ concentrations are high in the winter. However, the late summer and early fall also contribute significantly to the exceedances of the annual $PM_{2.5}$ standard when ozone levels are high. Utility loads are also at their highest during this time period. This study examines the possibility of controlling the two pollutants together during the late summer and early fall period by applying the US EPA's CMAQ photochemical air quality model to central California for the August-September period of years 2000 and 2005.

Higher 24-h $PM_{2.5}$ with two-month averages greater than 15 ug/m^3 is located mainly in the San Joaquin Valley near high ammonia emission sources. $PM_{2.5}$ concentrations have sharp spatial gradients that decrease quickly in the direction toward the Sierra Mountains to the east or coastal ranges to the west. In contrast, higher ozone concentrations have greater spatial extent and smaller gradients.

Ozone and $PM_{2.5}$ are negatively associated on an hourly basis largely due to opposite effects of their diurnal variations on relative humidity and temperature. However, on daily timescales, 8-h ozone maxima and 24-h average $PM_{2.5}$ are positively associated because both are sensitive to PBL height, which provides a measure of atmospheric stagnation. Such findings indicate that higher ozone and $PM_{2.5}$ tend to occur together during late summer and early fall under more stagnant conditions, and emphasize the importance of considering the control of the two pollutants, in concert.

Particulate nitrates are the main secondary component in $PM_{2.5}$ mass. At high PM locations (i.e. two-month average 24-h $PM_{2.5}$ > 15 ug/m^3), the formation chemistry of particulate NH_4NO_3 is limited by the availability of HNO_3.

Nitric acid formation is coupled to ozone chemistry by sharing the same precursors (NOx and AVOC). The chemical coupling of PM and ozone is investigated by simulating responses of the two pollutants to their common precursor emissions over two episodes representative of ventilated and stagnant conditions, respectively. Both concentrations and their sensitivities to precursor emissions of the two pollutants are greater in magnitude under the more stagnant conditions. Fine particulate matter ($PM_{2.5}$) sensitivities are dominated by sensitivities of particulate NH_4NO_3 to NOx. Therefore, the formation of HNO_3 is limited by NO_x and NO_x control is found to be most effective for controlling particulate NH_4NO_3.

At high PM locations, higher ozone levels (>75 ppb) during the more stagnant episode can also benefit from NOx control, but in general, ozone and PM largely show opposite responses to NOx for the emissions considered here (year 2000 and year 2005). However, as emissions are reduced further (~15 percent for stagnant conditions and ~30 percent for ventilated conditions from the year 2005 level), NO_x control, on average, becomes beneficial for both pollutants. If

very strict NOx reductions (greater than 30 percent) were to be required, both pollutants could be reduced. Although this would be difficult to achieve initially, the payoff in the future would be considerable.

GLOSSARY

ACM2	Asymmetric Convective Model version 2
AdjGR	Adjust Gas Ratio
AERONET	Aerosol Robotic NETwork
AEROS	Aerosol Module Version 5
AIRS	Aerometric Information Retrieval System
AQS	Air Quality System
ARB	Air Resources Board
AVOC	Anthropogenic Volatile Organic Compounds
BCON	Boundary Condition
BVOC	Biogenic Volatile Organic Compounds
CASTNet	Clean Air Status and Trends Network
CMAQ	Community Multiscale Air Quality
cor	Correlation Coefficient
CRPAQS	California Regional Particulate Air Quality Study
EC	Elemental Carbon
FRM	Federal Reference Method
HNO_3	Nitric Acid
IMPROVE	Interagency Monitoring of Protected Visual Environment
MBTU	Methlybutanol
MC	Mountain Counties
MdnB	Median Bias
MdnE	Median Error
NCC	North Central Coast
NDDN	National Dry Deposition Network
NH_3	Ammonia
NH_4^+	Ammonium
NH_4NO_3	Ammonia Nitrate
NMdnE	Normalized median Error
NO	Nitric Oxide
NO_3^-	Nitrate
NOAA	National Oceanic and Atmospheric Administration
NOx	Nitrogen Oxides
NWS	National Weather Service
O_3	Ozone
OC	Organic Carbon
OLE1	Olefin 1
PBL	Planetary boundary layer
pcor	Partial Correlation Coefficient
PM	Particulate matter
$PM_{2.5}$	Particle matter particulates less than 2.5 microns in aerodynamic diameter
POA	Primary Organic Aerosol

RH	Relative Humidity
RMSE	Root Mean Square Error
SARMAP	San Joaquin Valley Regional Modeling Adaptation Project
SARPRC99	State Air Pollution Research Center chemical mechanism produced in year 1999
SCC	South Central Coast
SFB	San Francisco Bay Area
SJV	San Joaquin Valley
SJVUAPCD	San Joaquin Valley Unified Air Pollution Control District
SO_2	Sulfur Dioxide
SO_4^{2-}	Sulfate
SOA	Secondary organic aerosol
SOx	Sulfur Oxides
STN	Speciation Trends Network
SV	Sacramento Valley
TC	Total Carbon
US EPA	United States Environmental Protection Agency
VOC	Volatile Organic Compound

REFERENCES

Appel, K. W., P. V. Bhave, et al. (2008). Evaluation of the community multiscale air quality (CMAQ) model version 4.5: Sensitivities impacting model performance; Part II - particulate matter. *Atmospheric Environment* **42**(24): 6057-6066.

Bao, J.-W., Michelson, S.A., Persson, P.O.G., Djalalova, I.V. and Wilczak, J.M. (2008) Observed and WRF-Simulated Low-Level Winds in a High-Ozone Episode during the Central California Ozone Study. Journal of Applied Meteorology and Climatology, Vol. 47, pp. 2372-2394.

Byun, D., and K.L. Schere (2006) Review of the Governing Equations, Computational Algorithms, and Other Components of the Models-3 Community Multiscale Air Quality (CMAQ) Modeling System. Applied Mechanics Reviews 59:51-77.

Carlton, A. G., P. V. Bhave, et al. (2010). Model Representation of Secondary Organic Aerosol in CMAQv4.7. *Environmental Science & Technology* **44**(22): 8553-8560.

Chow, J.C., Chen, L.-W. Antony, Watson, J.G., Lowenthal, D.H., Magliano, K.A., Turkiewicz, K. and Lehrman, D.E. (2006) PM2.5 chemical composition and spatiotemporal variability during the California Regional PM10/PM2.5 Air Quality Study (CRPAQS). Journal of Geophysical Research, Vol. 111, D10S04, pp. 1-17.

Davis, J. M., P. V. Bhave, et al. (2008). Parameterization of N2O5 reaction probabilities on the surface of particles containing ammonium, sulfate, and nitrate. *Atmos. Chem. Phys.* **8**(17): 5295-5311.

Foley, K. M., S. J. Roselle, et al. (2010). Incremental testing of the Community Multiscale Air Quality (CMAQ) modeling system version 4.7. *Geoscientific Model Development* **3**(1): 205-226.

Grell, G. A., J. Dudhia, et al. (1994). A description of the fifth-generation Penn State/NCAR mesoscale model (MM5). NCAR Technical Note, NCAR/TN-398+STR, 122 pp., NCAR, Boulder, CO, 1994.

Kelly, J. T., P. V. Bhave, et al. (2009). Simulating emission and chemical evolution of coarse sea-salt particles in the Community Multiscale Air Quality (CMAQ) model. *Geoscientific Model Development* **2**(2): 1335-1374.

Jin, L., N. J. Brown, et al. (2010). Seasonal Versus Episodic Performance Evaluation for an Eulerian Photochemical Air Quality Model. *JOURNAL OF GEOPHYSICAL RESEARCH* **115**: D09302.

Jin, L., S. Tonse, et al. (2008). Sensitivity Analysis of Ozone Formation and Transport for a Central California Air Pollution Episode. *Environ. Sci. Technol.* **42**(10): 3683-3689.

Jin, L., R. A. Harley, et al. (2011). Ozone pollution regimes modeled for a summer season in California's San Joaquin Valley: A cluster analysis. *Atmospheric Environment* **45**(27): 4707-4718.

Jin, L., A. Loisy, N. J. Brown, (2012). Role of meteorological processes in ozone responses to emission controls in California's San Joaquin Valley. *Journal of Geophysical Research*. Submitted.

Lunden, M. M., D. R. Black, et al. (2006). Characteristics of fine particle growth events observed above a forested ecosystem in the Sierra Nevada Mountains of California. *Aerosol Science and Technology* **40**(5): 373-388.

Michelson, S. A., I. V. Djalalova, et al. (2010). Evaluation of the Summertime Low-Level Winds Simulated by MM5 in the Central Valley of California. *Journal Of Applied Meteorology And Climatology* **49**(11): 2230-2245.

Minejima, C., Wooldridge, P.J. and Cohen, R.C. (2009) Is NO3/NO2O5 chemistry a source of aerosol HNO3 in the San Joaquin Valley? Poster presented at Fall AGU Meeting in San Francisco, CA, Dec. 14-18, 2009.

Nenes A, Pandis SN, Pilinis C (1998). ISORROPIA: A new thermodynamic equilibrium model for multiphase multicomponent inorganic aerosols, Aquat. Geoch., 4, 123-152.

Pinder, R. W., R. L. Dennis, et al. (2008). Observable indicators of the sensitivity of PM2.5 nitrate to emission reductions - Part I: Derivation of the adjusted gas ratio and applicability at regulatory-relevant time scales. *Atmospheric Environment* **42**(6): 1275-1286.

Tesche, T. W., R. Morris, et al. (2006). CMAQ/CAMx annual 2002 performance evaluation over the eastern US. *Atmospheric Environment* **40**(26): 4906-4919.

Weaver, C. P., E. Cooter, et al. (2009). A Preliminary Synthesis of Modeled Climate Change Impacts on U.S. Regional Ozone Concentrations. *Bulletin of the American Meteorological Society* **90**(12): 1843-1863.

APPENDIX A:
Emission Quality Checking and Processing

1. Emission files obtained from ARB.

A brief description of the emissions files obtained from ARB is provided in Table A-1.

Table A-1. Emission files documentation.

Emis Year	Descriptions	Notes
2000a	Seasonal project gas phase emissions: gridded emissions provided for area, mobile, biogenic; and point sources are lofted according to MM5 meteorology.	1. Day of week difference in anthropogenic emissions, and day-specific biogenic emissions. 2. MBTU emissions are not included
2000b	Both gas phase and PM emissions are provided in two categories: gridded surface emissions and individual point sources. Point source needs to be lofted according to MM5 meteorology.	1. Scaled from base year 1998 inventory. 2. MBTU is lumped into OLE1. 3. The spatial resolution appears to be coarser than the gridded emissions of year 2005. 4. Emissions are day specific, although anthropogenic emissions have similar weekly cycles.
2005	Both gas phase and PM emissions, provided in two categories: gridded surface emissions and individual point sources. Point source can be lofted according to MM5 meteorology.	1. Scaled from base year 2002 inventory. 2. MBTU is lumped into OLE1. 3. Emissions are day specific, although anthropogenic emissions have similar weekly cycles.

In processing emissions for year 2000, to avoid the spatial resolution issues (Table A-1), we combined 2000a gas phase emissions (no ammonia (NH3) emissions) and 2000b PM and NH3 emissions. For the July 25 to August 8 modeling period, the daily total emissions are shown in Table A-2. Note that days 211 and 212 are Saturday and Sunday, respectively.

Table A-2. Daily total emissions of year 2000 (tonnesday) showing for a two-week period.

	NOx	AVOC	BVOC	CO	NH3	PM25	PM10	SOx	PMother	PSO4	POA	PEC
207	1513	1386	716	6820	453	245	911	128	137	14	73	21
208	1513	1385	575	6820	453	245	911	128	137	14	73	21
209	1513	1384	483	6820	453	245	911	128	137	14	73	21
210	1586	1408	611	7115	453	246	913	128	138	14	73	21
211	1232	1435	705	7277	453	218	822	126	126	15	58	20
212	1157	1407	772	7038	453	215	819	126	125	15	55	19
213	1513	1388	874	6820	453	245	912	128	137	14	73	21
214	1513	1388	945	6820	452	241	882	128	132	14	74	21
215	1513	1388	857	6820	452	241	882	128	132	14	74	21
216	1513	1386	657	6820	452	241	882	128	132	14	74	21
217	1586	1408	583	7115	452	242	884	128	132	14	74	21
218	1232	1434	632	7277	452	213	792	126	120	15	58	20
219	1157	1406	586	7038	452	210	789	126	120	15	56	20
220	1513	1384	454	6820	452	241	883	128	132	14	74	21

For year 2005 simulations, the days of week are aligned with that of year 2000 to facilitate the comparison. Note here, the Julian dates are automatically aligned: for example, day 211 in 2005 (July 28th) is a Saturday, same as day 211 in 2000 (July 29th).

The actual emissions for year 2005 for the modeling period have almost doubled AVOC emissions as those for the year 2000. This is due to the fact that ARB has lumped a large amount of biogenic MBTU emissions into OLE1 for the 2005 emission input, while it consisted of only anthropogenic sources for the year 2000. MBTU was not included in the 2000 emission input, so to be consistent, we have manually removed MBTU from the OLE1 emissions. The new OLE1 emissions of year 2005 are estimated by scaling the 2000 OLE1 emissions by 0.79. This scaling factor was derived from the emission sums (with biogenic emissions removed) of year 2000 and 2005 provided by Bruce Jackson.

Since the purpose of this study is to isolate the effects of anthropogenic emission changes on air quality, the 2005 biogenic emissions are replaced with year 2000 biogenic emissions.

Table A-3. Daily emission totals of year 2005, after corrections are made to the biogenic and OLE1. (tonnes/day), are provided for a two-week period.

	NOx	AVOC	BVOC	CO	NH3	PM25	PM10	SOx	PMother	PSO4	POA	PEC
207	1316	1264	716	4898	446	268	912	138	140	14	89	24
208	1315	1260	575	4877	446	268	912	138	140	14	89	24
209	1318	1256	483	4850	446	268	912	138	140	14	89	24
210	1332	1287	611	5130	446	269	914	139	141	15	89	24
211	1013	1288	705	5426	446	248	828	133	130	17	77	24
212	951	1273	772	5279	446	246	825	132	130	17	76	24
213	1305	1261	874	4786	445	247	861	132	132	14	78	22
214	1320	1252	945	4738	445	246	861	131	132	14	78	22
215	1313	1251	857	4739	445	246	861	131	132	14	78	22
216	1307	1254	657	4761	445	246	861	131	132	14	78	22
217	1327	1292	583	5085	445	248	863	132	133	14	78	23
218	1014	1288	632	5337	445	225	775	128	121	16	66	22
219	951	1268	586	5162	445	223	772	127	121	16	64	22
220	1299	1252	454	4743	445	247	861	132	132	14	78	22

When 2005 emissions are compared to those of year 2000, NOx emissions are reduced by 13~18percent depending on the day of week and AVOCs are also reduced by ~10percent. In contrast, PM emissions increased in 2005, especially for ()POA (~20-35percent) and PEC() (~15-20percent) in the month of July. Spatially, the differences are largest in the northern parts of Fresno or Tuolumne counties in the San Joaquin Valley (SJV), and depend on the month, and in the north central Coast air basin (Figure A-1). Note that the roadways are obvious in the ()OA emission difference maps, which could be an artifact of the relatively coarser resolution of year 2000 emissions (emissions are more spread out). Figure A-2 provides an example of this for day 211. The Year 2000 emission map resembles an interpolation from a coarser resolution map, and the emissions along the roadways are located in more grids, which reduces the emissions in individual grids.

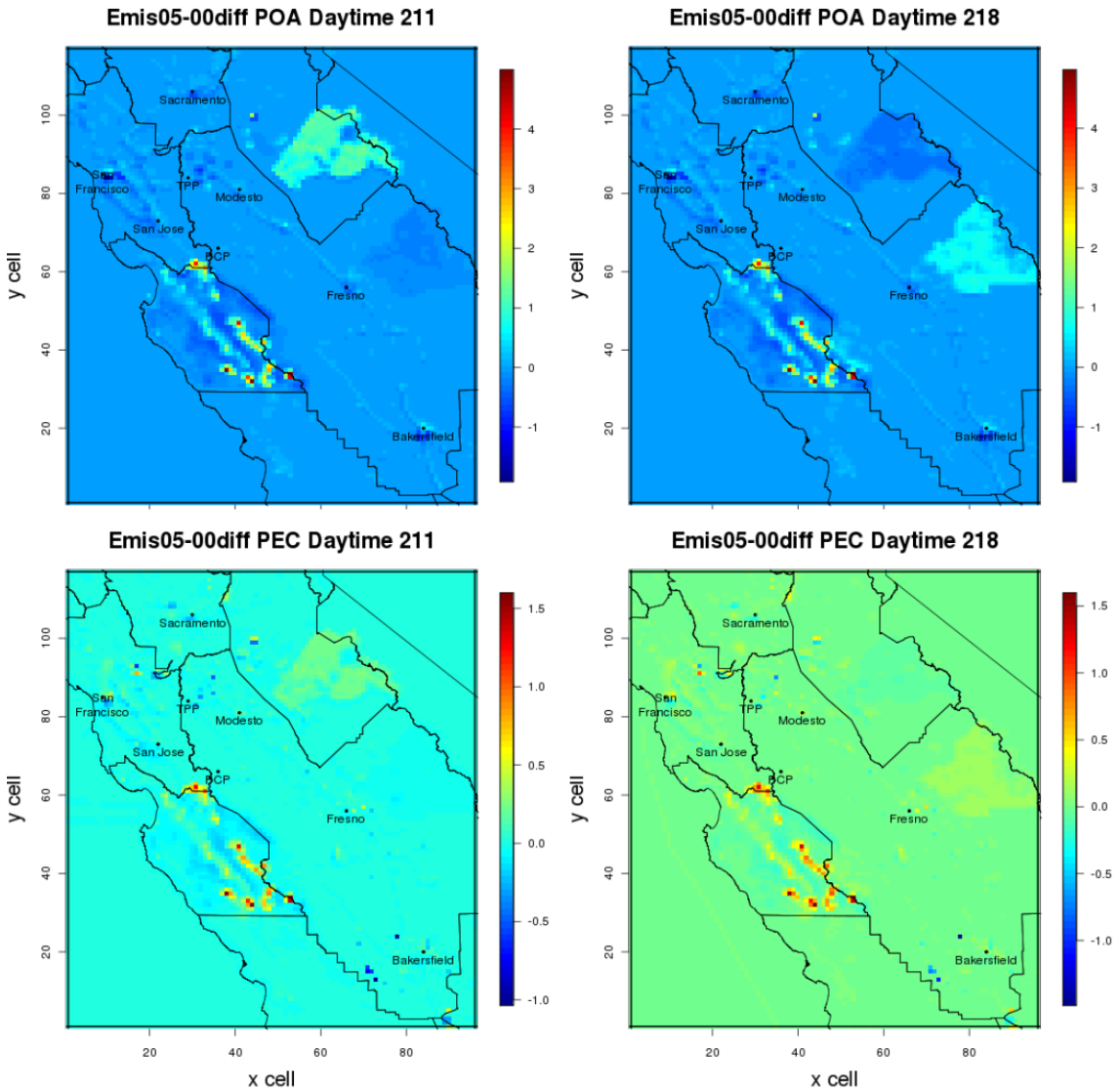

Figure A-1. OA and EC emission rate differences (g/s) between year 2005 (top) and year 2000 (bottom).

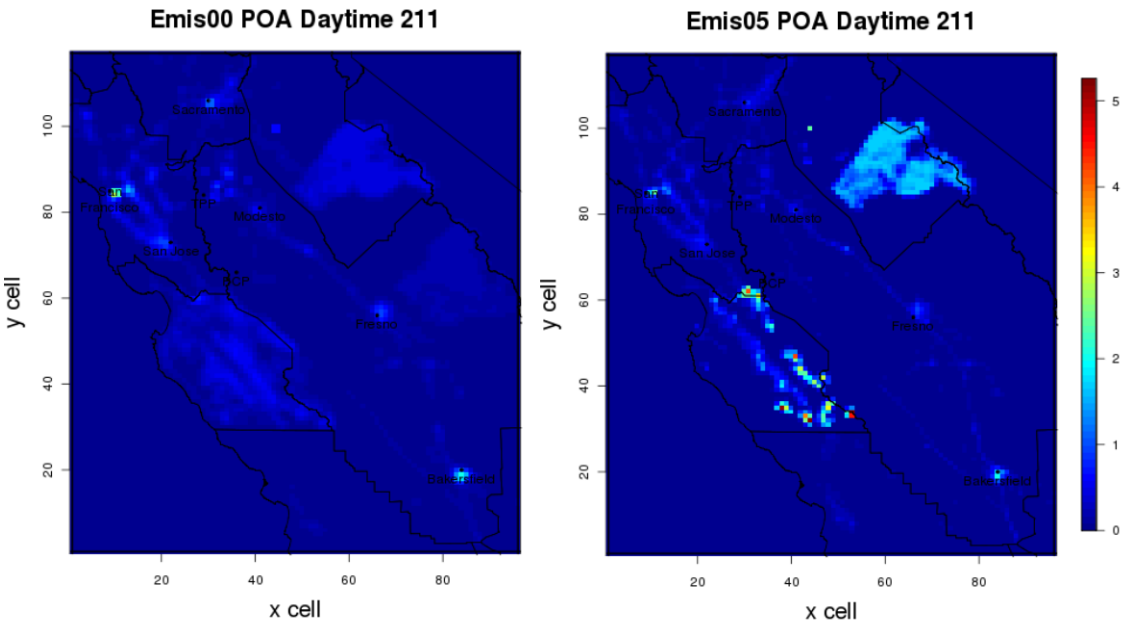

Figure A-2. An illustration of the spatial resolution differences between 2000 (left) and 2005 (right), emission rates in g/s.

According to Bruce Jackson of ARB, the base year differences may explain the most prominent spatial patterns in Figures A-1, and A-2. Emissions from 2000 and 2005 are respectively, scaled from base years 1998 and 2002, and their emission factors and species profiles may be inconsistent. For example, the 2005 emissions reflect overnight heating in Tuolumne County (Yosemite) ending in July, while the 2000 emissions continued this through August. These emission characteristics may not reflect the reality.

2. Emission processing programs

In addition to the script and programs documented before, the following programs were written to process the 2005 emissions.

- Cshell script 'ptem.JulyAug05.csh': to loop through the modeling period and loft daily 2005 point source emissions according to year 2000 day of week.
- Cshell script 'proc.arem05': to loop through the modeling period and call 'proc.carb.exe', and 'changeyear.exe' to process the gridded surface emissions
- Fortran program 'fake.emis.exe': to replace biogenic emissions in 2005 with those in 2000, and replace OLE1 with the estimated values by scaling anthropogenic OLE1 in 2000.
- Fortran program 'emis_merge.sarmap.JulAug05.exe': to merge the lofted point source emissions with gridded surface emissions processed earlier.

APPENDIX B:
Lateral Chemical Boundary Conditions

We obtained 2000 July BCON for the 12km x 12km California domain with 15 vertical layers used in ARB PM modeling. The values in this BCON file are based on MOZART (version 2) output in the California domain (personal communication with Jeremy Avise at ARB). We developed procedures for processing the ARB boundary conditions into the 4km x 4km SARMAP domain boundary conditions with 27 vertical layers. The procedures include obtaining the four boundary vertical profiles for individual species, vertical linear interpolation of the 15 vertical layers into SARMAP 27 vertical layers according to the pressure levels, and modifying the western and southern boundaries to reflect land/ocean differences.

We also compared the new boundary conditions and the old ones used in our seasonal project for select species. Additional boundary values based on a more recent literature review were also considered.

1. Domain size

The ARB California domain (from which we obtained our boundary conditions), the CCOS domain and the SARMAP domain are show on the map below after all being converted according to the SARMAP projection origins, as seen below in Figure B-1. This study used SARMAP domain.

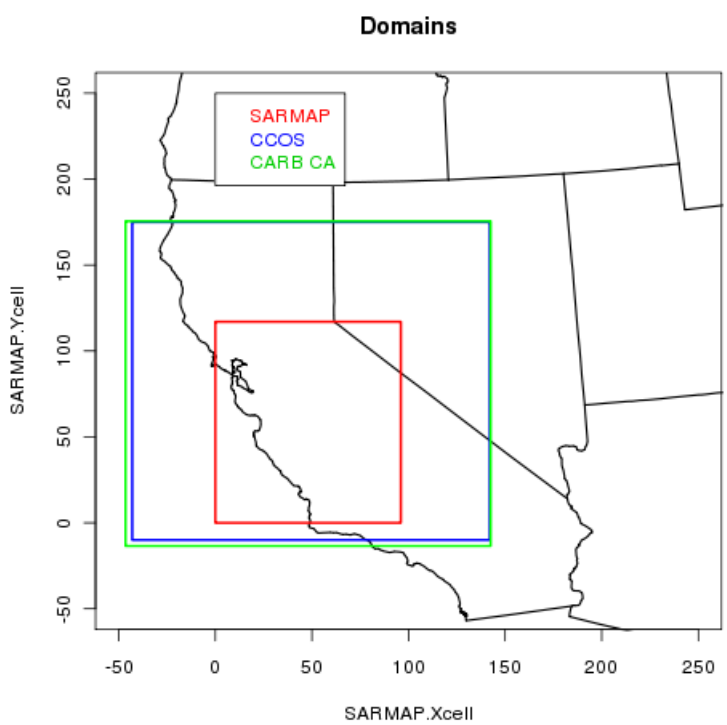

Figure B-1 Different modeling domains.

The ARB domain is similar in size and location to the CCOS domain. In the two larger domains, the western boundary is the Pacific Ocean, while the smaller SARMAP domain has a portion of the western boundary over land.

2. Vertical Structure of the boundary conditions

There are 15 vertical layers in the ARB boundary conditions with pressure levels indicated below:

1.f, 0.9958f, 0.9907f, 0.9846f, 0.9774f, 0.9688f, 0.9585f, 0.9463f, 0.9319f, 0.9148f, 0.8946f, 0.8709f, 0.8431f, 0.7301f, 0.4954f, 0.f

Note the first layer has pressure f, and each vertical layer's pressure is given as a fraction of the pressure at the surface. For each layer, the boundary conditions are homogeneous on its sides.

The CCOS and SARMAP domains have 27 vertical layers with more layers near the surface:

1.f, 0.9969f, 0.9935f, 0.9899f, 0.9861f, 0.9821f, 0.9777f, 0.9731f, 0.9682f, 0.9573f, 0.9382f, 0.924f, 0.9088f, 0.8925f, 0.8752f, 0.8471f, 0.8141f, 0.7863f, 0.7531f, 0.7135f, 0.6123f, 0.506f, 0.3656f, 0.2558f, 0.1339f, 0.0804f, 0.0362f, 0.f

Vertical linear interpolation is performed to translate the ARB domain to the SARMAP domain.

The vertical profiles of the four boundaries for select species are plotted in Figures B-2and B-3 below.

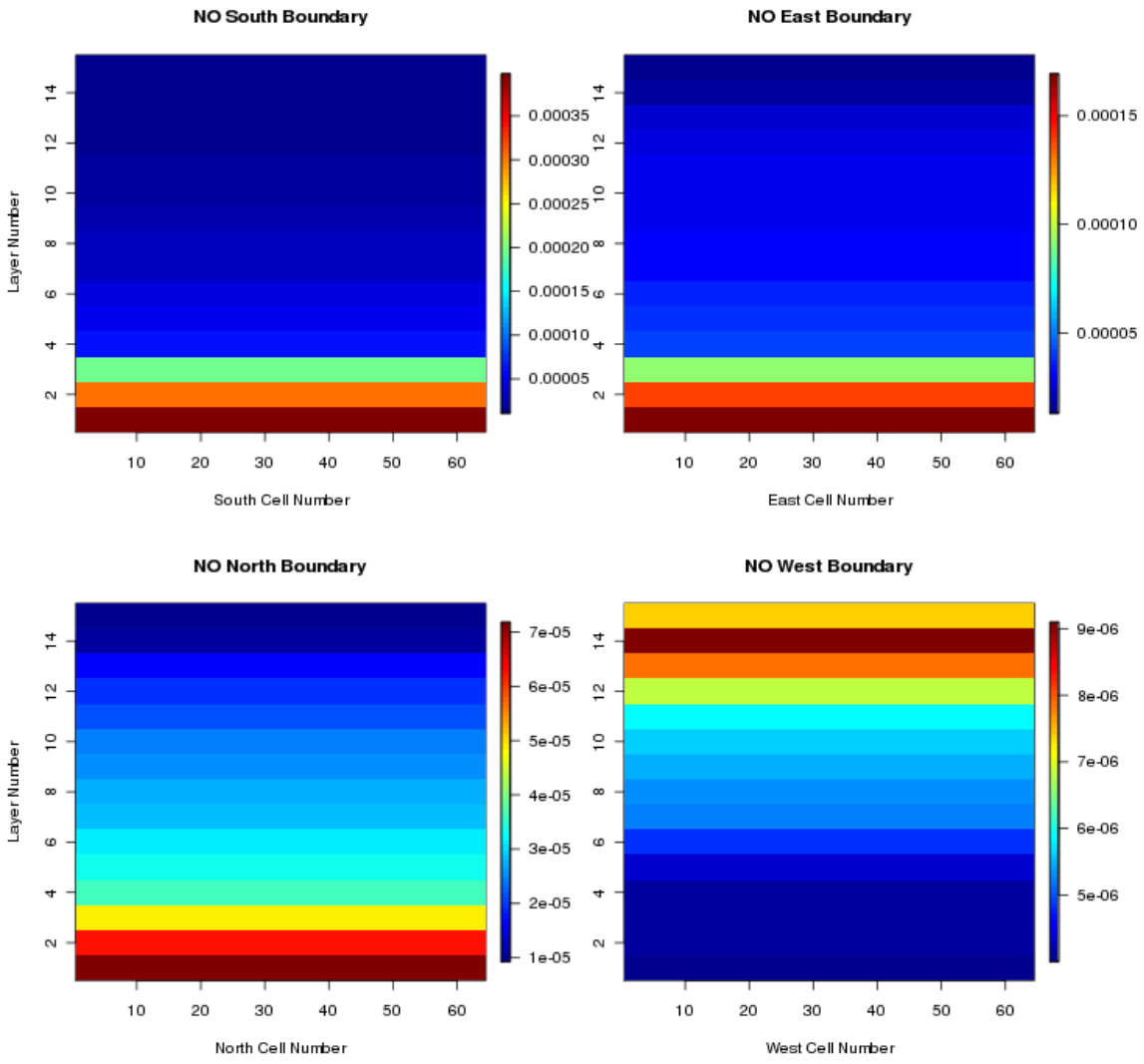

Figure B-2 SARMAP boundary conditions (vertically interpolated from ARB boundary conditions) for NO

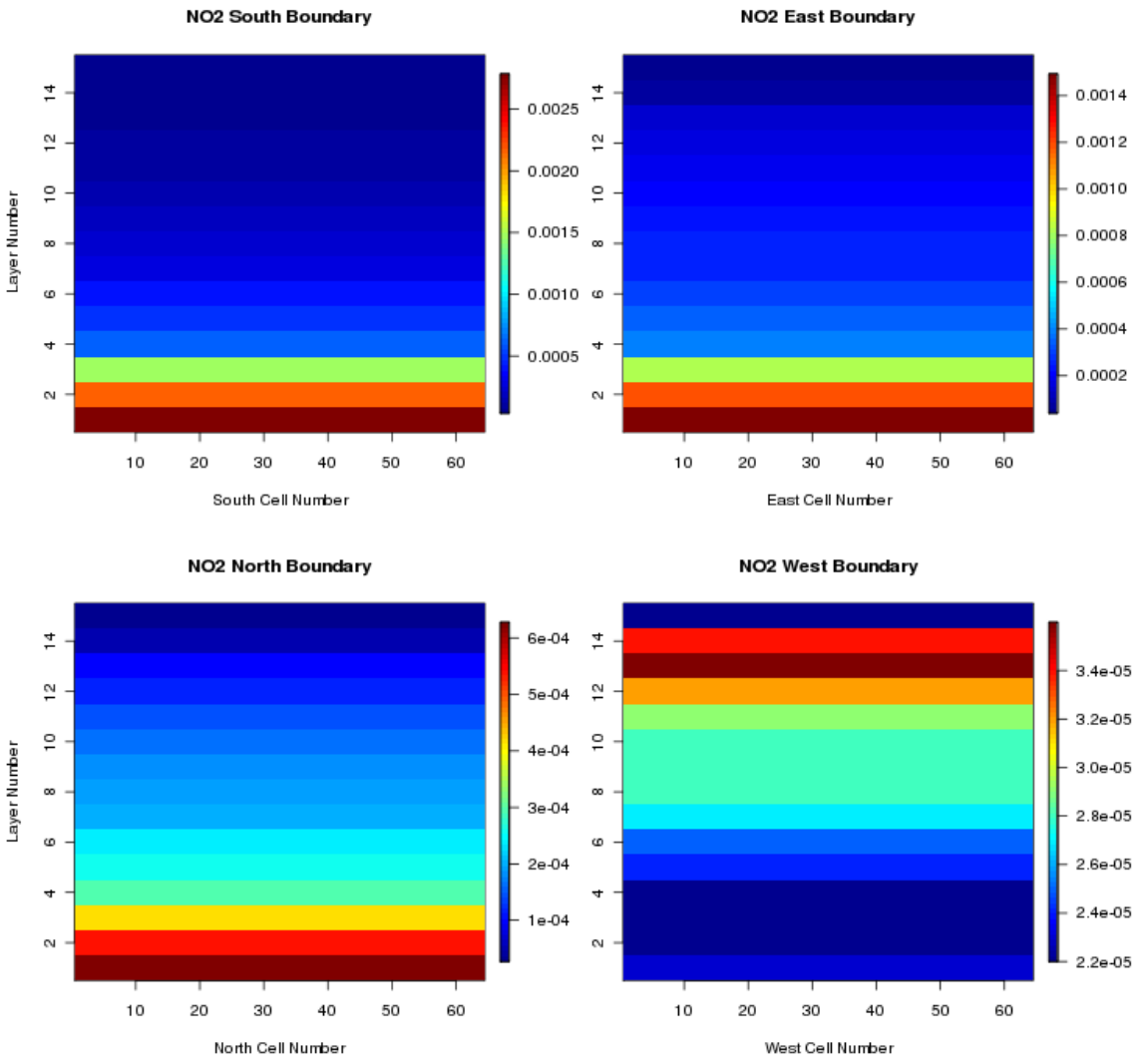

Figure B-3 SARMAP boundary conditions (vertically interpolated from ARB boundary conditions) for NO

3. Assign northern boundary values to the land portion of the SARMAP western boundary, and an ocean value to the ocean portion of the southern boundary

The northern part of SARMAP western boundary is over land; hence the ocean values are not appropriate. We use the northern (boundary conditions) BCON values for this part as illustrated in the following figure. Also, part of the southern boundary is over the Pacific Ocean; values were modified using the western ocean BC.

The figure on the right is modified from the figure on the left (Figure B-4), with the land portion of the western boundary conditions modified to use the northern BCON values, and ocean part of the southern boundary conditions is modified to use the western BCON values.

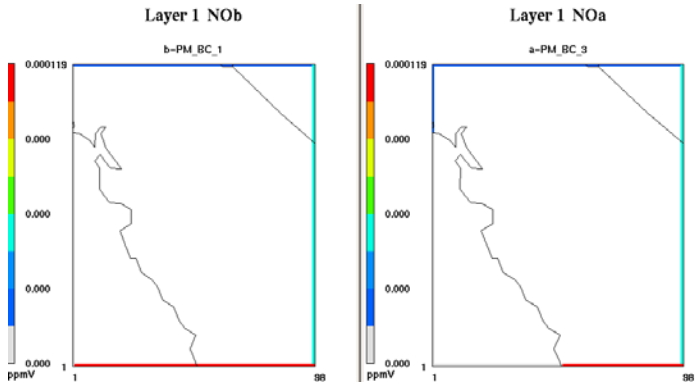

Figure B-4 Modification of western boundary conditions in the land portion.

4. Comparison to the NO BCON used in the seasonal project

Table B-1 Boundary conditions used for previous project for the modeling domain

Species	Seasonal Project Western BC (ppb)	MOZART derived Western BC (ppb)
CO	120 (Goldstein 2004)	77
NO	0.01 (Nowak 2004)	0.004
NO2	0.03 (Nowak 2004)	0.02
PAN	0.15 (Nowak 2004)	0.016
PAN2	0.02 (Nowak 2004)	0.004 (MA_PAN)
O3 at sfc	22 (Newchurch 2003)	22
O3 at 1km (layer15)	44 (Newchurch 2003)	39.6
O3 at 2km (layer18)	60 (Newchurch 2003)	44
O3 at 3km (layer20)	60 (Newchurch 2003)	49.4
MEOH	0.88 (Singh 2001)	0.42
HCHO	0.3 (Singh 2001)	0.2
CCHO	0.15 (Singh 2001)	0.017
ACETONE	0.89 (Nowak 2004)	0.52
ALKANE-1	1.06 (Nowak 2004)	0.47
ALKANE-2	0.13 (Nowak 2004)	0.025
AROMATIC-1	0.019 (Nowak 2004)	NA
AROMATIC-2	0	NA
ISOPRENE	0	4.3E-5
OLEFIN-1	0	0.016
OLEFIN-2	0	NA

The new western BC has lower values of concentration, but the surface ozone is identical.

The table below allows a comparison of the current N/E/S BC used in the previous seasonal modeling project to those derived from MOZART and used currently.

Table B-2 Comparison of BCs over the ocean in the previous seasonal modeling project to those used in the current study

Species	Seasonal Project N/E/S BCON (ppb)	MOZART derived N/E/S BCON (ppb)
CO	200	120/150/150
NO	0.05	0.07/0.17/0.4
NO2	1	0.63/1.5/2.8
PAN	0.005	0.24/0.15/0.45
PAN2	0	0.19/0.063/0.19 (MA_PAN)
O3 at sfc	40	39/53/42
O3 at 1km (layer15)	48	55/64/57
O3 at 2km (layer18)	60	57/64/59
O3 at 3km (layer20)	60	60/66/62
MEOH	NA	4.5/8.2/1.2
HCHO	2	2.1/1.8/1.7
CCHO	0.456	0.089/0.062/0.09
ACETONE	1	0.7/0.75/0.98
ALKANE-1	10	0.64/0.68/0.65
ALKANE-2	2.5	0.077/0.1/0.12
AROMATIC-1	0.35	NA
AROMATIC-2	0.25	NA
ISOPRENE	0.1	0.12/0.056/0.053
OLEFIN-1	0.5	0.14/0.096/0.086

OLEFIN-2	0.2	NA

The MOZART BCONs are also generally lower (significantly lower for ALK1 and ALK2) except for PAN for the other three boundaries.

The highest MOZART VOCs on the other three boundaries is MEOH, instead of ALK1, ALK2 which were quite high in the previous seasonal study. Methanol is the second most abundant organic molecule in the atmosphere after methane (Singh et al. 2001) and is the predominant oxygenated organic compound in the mid to upper troposphere (Heikes et al. 2002), which is reflected in the western BCON. It is primarily emitted from biogenic sources (according to the ARB data) and anthropogenically, its emissions result from its use as a solvent etc.

5. MOZART PM BC conditions

The lateral boundary conditions of the PM species include:

ASO4J ASO4I ANH4J ANH4I ANO3J ANO3I AORGPAJ AORGPAI AECJ AECI NUMATKN NUMACC NUMCOR SRFATKN SRFACC

Note: "A" designates aerosol mass, "NUM" designates aerosol number, "SRF" designates surface area. "I" designates i-mode, the smaller nuclei or Aitken nuclei, represents fresh particles either from nucleation or from direct emissions; "J" designates the j-mode, the larger (accumulation mode) and aged particles. Units: microgram/m^3, #/m^3, m^2/m^3 for gas, PM mass, number concentration, and surface area, respectively. These are shown for the various entities in the Table B-3 below for the four boundaries. Explanation of the species name is in Table B4.

Table B-3 Lateral boundary conditions for particulate matter species.

Surface BCON	**Western**	**Northern**	**Eastern**	**Southern**
ASO4J	1.10E+00	1.20E+00	1.20E+00	1.50E+00
ASO4I	5.70E-02	6.30E-02	6.50E-02	8.10E-02
ANH4J	4.00E-01	4.50E-01	4.60E-01	5.80E-01
ANH4I	2.10E-02	2.40E-02	2.40E-02	3.10E-02
ANO3J	9.10E-04	5.32E-03	1.00E-02	9.59E-03
ANO3I	4.80E-05	2.81E-04	5.52E-04	5.00E-04
AORGPAJ	1.60E-01	2.59E+00	4.18E+00	1.90E+00
AORGPAI	8.20E-03	1.40E-01	2.19E-01	9.98E-02
AECJ	3.50E-02	2.50E-01	4.29E-01	4.79E-01

AECI	1.90E-03	1.30E-02	2.29E-02	2.49E-02
NUMATKN	1.00E+06	1.00E+06	1.00E+06	1.00E+06
NUMACC	4.10E+05	4.10E+05	4.10E+05	4.10E+05
NUMCOR	2.70E+02	2.70E+02	2.70E+02	2.70E+02
SRFATKN	4.90E-09	4.90E-09	4.90E-09	4.90E-09
SRFACC	3.00E-07	3.00E-07	3.00E-07	3.00E-07

Table B4 Explanation of PM species names used in the model

Species Name	**Explanation**	**Unit**
ASO4J	Sulfate aerosol in J mode	microgram/m^3
ASO4I	Sulfate aerosol in i mode	microgram/m^3
ANH4J	Ammonium aerosol in J mode	microgram/m^3
ANH4I	Ammonium aerosol in i mode	microgram/m^3
ANO3J	Nitrate aerosol in J mode	microgram/m^3
ANO3I	Nitrate aerosol in i mode	microgram/m^3
AORGPAJ	Organic aerosol in J mode	microgram/m^3
AORGPAI	Organic aerosol in I mode	microgram/m^3
AECJ	Elemental carbon in J mode	microgram/m^3
AECI	Elemental carbon in i mode	microgram/m^3
NUMATKN	Number concentration in Aiken model	#/m^3
NUMACC	Number concentration in accumulation mode	#/m^3
NUMCOR	Number concentration in coarse mode	#/m^3
SRFATKN	Surface area in Aiken mode	m^2/m^3
SRFACC	Surface area in accumulation mode	m^2/m^3

Goldstein, A. H., Dylan B. Millet, Megan McKay, Lyatt Jaegle´, Larry Horowitz, Owen Cooper, Rynda Hudman, Daniel J. Jacob, Sam Oltmans, and Andrew Clarke (2004), Impact of Asian emissions on observations at Trinidad Head, California, during ITCT 2K2, J. Geophys. Res., 109, doi:10.1029/2003JD004406.

Heikes, B. G., et al., (2002). Atmospheric methanol budget and ocean implication, *Global Biogeochem. Cycles*, 16(4), 1133, doi:10.1029/2002GB001895.

Newchurch, M.J. et al. (2003), Vertical distribution of ozone at four sites in the United States. J. Geophys. Res. **108(**D1), 4031: doi: 10.1029/2002JD002059

Nowak, J. B., D. D. Parrish, J. A. Neuman, J. S. Holloway, O. R. Cooper, T. B. Ryerson, J. D.K. Nicks, F. Flocke, J. M. Roberts, E. Atlas, J. A. d. Gouw, S. Donnelly, E. Dunlea, G. H, L. G. Huey, S. Schauffler, D. T. Sueper, D. J. Tanner, C. Warneke, and F. C. Fehsenfeld (2004), Gas-Phase Chemical Characteristics of Asian Emission Plumes Observed During ITCT 2k2 Over the Eastern North Pacific Ocean, J. Geophys. Res., 109, doi:10.1029/2003JD004488.

Singh, H., Y. Chen, et al. (2001). Evidence from the Pacific troposphere for large global sources of oxygenated organic compounds. *Nature* **410**(doi:10.1038/35074067): 1078-1081.